

Supporting Information
Heteroporous bifluorenylidene-based covalent organic frameworks displaying exceptional dye adsorption behavior and high energy storage

Ahmed F. M. EL-Mahdy,^{a,b} Mohamed Barakat Zakaria,^{c,d,e} Hao-Xin Wang,^a Tao Chen,^f
Yusuke Yamauchi,^{c,e,g} and Shiao-Wei Kuo*^{a,h}

- ^a *Department of Materials and Optoelectronic Science, Center of Crystal Research, National Sun Yat-Sen University, Kaohsiung 80424, Taiwan.*
- ^b *Chemistry Department, Faculty of Science, Assiut University, Assiut 71516, Egypt.*
- ^c *JST-ERATO Yamauchi Materials Space-Tectonics Project and International Research Center for Materials Nanoarchitectonics (WPI-MANA), National Institute for Materials Science (NIMS), 1-1 Namiki, Tsukuba, Ibaraki 305-0044, Japan.*
- ^d *Department of Chemistry, Faculty of Science, Tanta University, Tanta, Gharbeya 31527, Egypt.*
- ^e *School of Chemical Engineering and Australian Institute for Bioengineering and Nanotechnology (AIBN), The University of Queensland, Brisbane, Queensland 4072, Australia.*
- ^f *Ningbo Institute of Material Technology and Engineering, Chinese Academy of Science, Zhongguan West Road 1219, 315201 Ningbo, China.*
- ^g *JST-ERATO Yamauchi Materials Space-Tectonics Project, Kagami Memorial Research Institute for Materials Science and Technology, Waseda University, 2-8-26 Nishiwaseda, Shinjuku, Tokyo 169-0051, Japan.*
- ^h *Department of Medicinal and Applied Chemistry, Kaohsiung Medical University, Kaohsiung 807, Taiwan.*

Corresponding authors:

Shiao-Wei Kuo, +886-7-5252000 ext 4079, E-mail: kuosw@faculty.nsysu.edu.tw

S1. Materials

Chemicals and solvents were obtained from commercial sources and used as received. Pyrene, tetrakis(triphenylphosphine)palladium(0), *n*-bromosuccinimide, and carbazole were purchased from Acros. Phenanthrene-9,10-dione, dibenzoyl peroxide, 4-bromoaniline, 4-formylphenylboronic acid, potassium permanganate, and Lawesson's reagent were obtained from Alfa Aesar. Bis(pinacolato)diboron, [1,1'-bis(diphenylphosphino)ferrocene]dichloropalladium(II), potassium hydroxide, sodium bisulfite, and potassium acetate were purchased from J. T. Baker. Bromine, nitrobenzene, sulfuric acid, and 4-aminophenylboronic acid pinacol ester were obtained from Sigma–Aldrich.

S2. Characterization

¹H and ¹³C NMR spectroscopy. NMR spectra were recorded using an INOVA 500 instrument, with DMSO-*d*₆ and CDCl₃ as solvents and tetramethylsilane (TMS) as the external standard. Chemical shifts are provided in parts per million (ppm).

Fourier transform infrared (FTIR) spectroscopy. FTIR spectra were recorded using a Bruker Tensor 27 FTIR spectrophotometer and the conventional KBr plate method; 32 scans were collected at a resolution of 4 cm⁻¹.

Solid state nuclear magnetic resonance (SSNMR) spectroscopy. SSNMR spectra were recorded at National Cheng Kung University using a Bruker Avance III HD solid state NMR spectrometer and a Bruker magic-angle-spinning (MAS) probe, running 32,000 scans.

Thermogravimetric analysis (TGA). TGA was performed using a TA Q-50 analyzer under a flow of N₂. The samples were sealed in a Pt cell and heated from 40 to 800 °C at a heating rate of 20 °C min⁻¹ under N₂ at a flow rate of 50 mL min⁻¹.

Powder X-ray diffraction (PXRD). PXRD was performed using a Siemens D5000 and monochromated Cu/Kα (λ = 0.1542 nm). The sample was spread in a thin layer on the square recess of an XRD sample holder.

Surface area and porosimetry (ASAP/BET). The BET surface areas and porosimetry measurements of the prepared samples (ca. 20–100 mg) were performed using a Micromeritics ASAP 2020 surface area and porosity analyzer. Nitrogen isotherms were generated through incremental exposure to ultrahigh-purity N₂ (up to ca. 1 atm) in a liquid N₂ (77 K) bath.

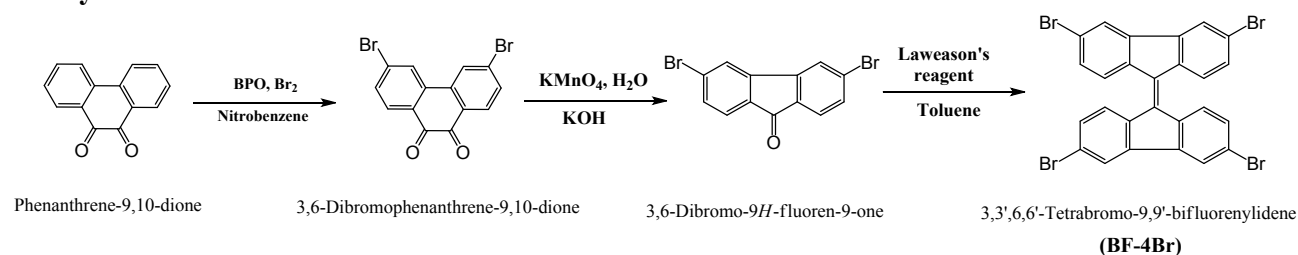
Field-emission scanning electron microscopy (FE-SEM). FE-SEM was conducted using a JEOL JSM-7610F scanning electron microscope. Samples were subjected to Pt sputtering for 100 s prior to observation.

Transmission electron microscopy (TEM). TEM was performed using a JEOL-2100 scanning electron microscope, operated at 200 kV.

COF structural simulations. Molecular modeling was performed using Reflex, a software package for crystal determination from XRD patterns. Unit cell dimensions were first determined manually from the observed XRD peak positions using the coordinates.

UV–Vis–NIR spectroscopy. UV–Vis–NIR spectra were recorded at 25 °C using a Jasco V-570 spectrometer, with deionized water as the solvent. Raman spectra were recorded at 25 °C using a Jobin–Yvon T6400 micro Raman apparatus, with a He–Cd laser (325 nm line) as an excitation source.

S3. Synthetic Procedures

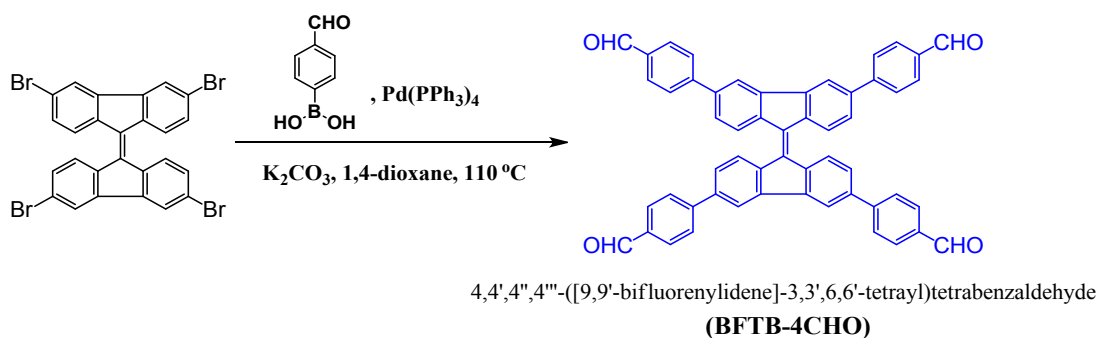


Scheme S1. Synthesis of 3,3',6,6'-tetrabromo-9,9'-bifluorenylidene (BF-4Br).

3,6-Dibromophenanthrene-9,10-dione: According to the reported method,^{S1} phenanthrene-9,10-dione (5 g, 24 mmol) and dibenzoyl peroxide (0.2 g, 0.83 mmol) were dissolved at room temperature in nitrobenzene (30 mL). Then, bromine (1.4 g, 8.7 mmol) was added dropwise to the reaction mixture and then heated at 110 °C. Further amount of bromine (6.9 g, 43.3 mmol) was added dropwise to the reaction mixture. After two hours heating, the reaction mixture was cooled and diluted with ethanol (30 mL) was added. The resultant solid was isolated by filtration and washed several times with ethanol. The product was then dried at 60 °C to yield 8.3 g (91% yield) 3,6-dibromophenanthrene-9,10-dione an orange powder. ¹H-NMR (500 MHz, DMSO-*d*₆) δ (ppm): 8.19 (d, *J* = 1.8 Hz, 2H), 7.93 (d, *J* = 6 Hz, 2H), 7.59 (dd, *J* = 6, 1.8 Hz, 2H). ¹³C NMR (125 MHz, DMSO-*d*₆) δ (ppm): 179.0, 136.2, 133.5, 132.2, 130.0, 127.7.

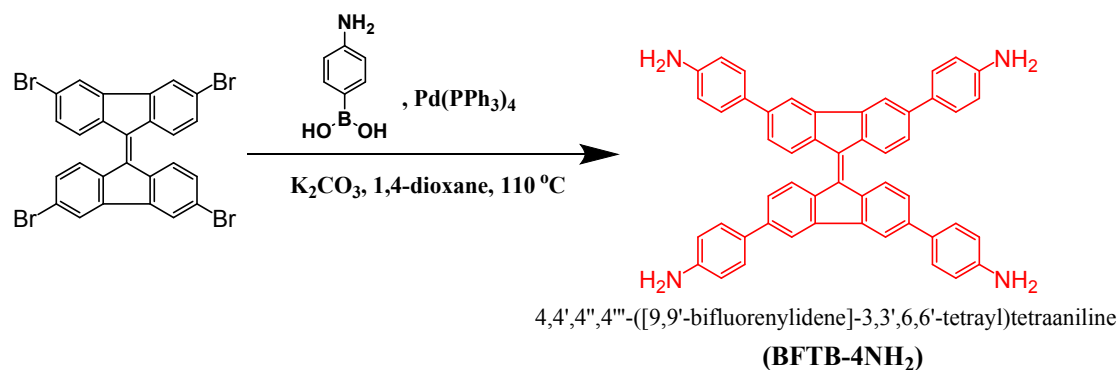
3,6-Dibromo-9H-fluoren-9-one: According to the reported method,^{S2} 3,6-dibromophenanthrene-9,10-dione (5 g, 13.6 mmol) was added to a solution of potassium hydroxide (8.15 g, 0.18 mol) dissolved in water (60 mL) and then heated to 130 °C. After two hours, potassium permanganate (11.43 g, 72.3 mmol) was added and the reaction mixture further heated at 130 °C for two hours. The mixture was cooled to room temperature and then neutralized with diluted sulfuric acid to pH = 7. Sodium bisulfite was added slowly until a complete precipitation of light-yellow solid. The resultant solid was filtered and washed several times with water. The product was then dried at 60 °C to yield 3.3 g (72% yield) 3,6-dibromo-9H-fluoren-9-one a light-yellow powder. ¹H-NMR (500 MHz, CDCl₃) δ (ppm): 7.68 (d, *J* = 1.8 Hz, 2H), 7.56 (d, *J* = 12 Hz, 2H), 7.51 (dd, *J* = 12, 1.8 Hz, 2H). ¹³C NMR (125 MHz, DMSO-*d*₆) δ (ppm): 193.8, 146.2, 133.4, 132.0, 130.1, 125.8.

3,3',6,6'-Tetrabromo-9,9'-bifluorenylidene (BF-4Br): A mixture of 3,6-dibromo-9H-fluoren-9-one (1 g, 2.96 mmol) and Lawesson's reagent (0.6 g, 1.483 mmol) in dry toluene (40 mL) was refluxed at 110 °C for 20 hours. After cooling, a precipitate was formed and isolated by filtration. The precipitate was heated in acetone for 10 minutes and then filtered again. The product was then dried at 60 °C to yield 0.33 g (35% yield) BF-4Br as an orange powder. The product was partially soluble in common organic solvent, so we performed H NMR spectroscopy only. ¹H-NMR (500 MHz, DMSO-*d*₆) δ (ppm): 8.66 (d, *J* = 1.8 Hz, 4H), 7.93 (d, *J* = 12 Hz, 4H), 7.77 (dd, *J* = 6, 1.8 Hz, 4H).



Scheme S2. Synthesis of 4,4',4'',4'''-(9,9'-bifluorenylidene)-3,3',6,6'-tetrayl)tetrabenzaldehyde (BFTB-4CHO).

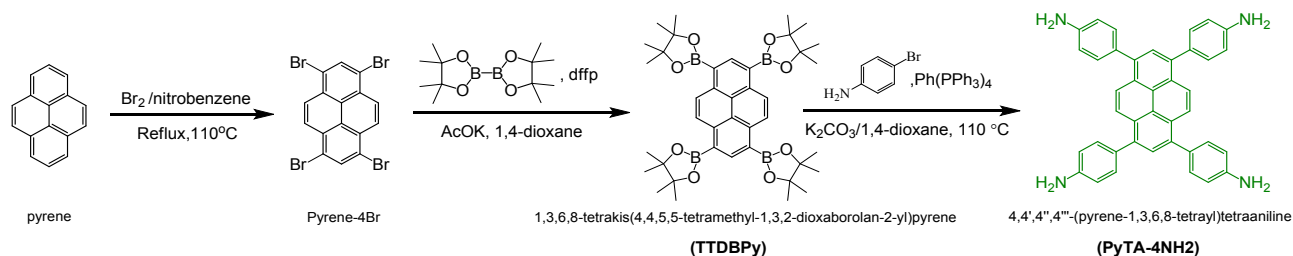
4,4',4'',4'''-(9,9'-bifluorenylidene)-3,3',6,6'-tetrayl)tetrabenzaldehyde (BFTB-4CHO): A 100 mL round-bottom flask was charged with BF-4Br (1 g, 1.55 mmol), 4-formylphenylboronic acid (1.86 g, 12.4 mmol), tetrakis(triphenylphosphine)palladium(0) 90 mg, 0.077 mmol), and potassium carbonate (2.15 g, 15.55 mmol). The solids were evacuated under high pressure for 15 minutes. Then, dioxane (50 mL) and water (10 mL) were added and the reaction mixture allowed to heat at 100 °C for 48 hours under N₂. After the consumption of BF-4Br, the reaction mixture was cooled to room-temperature and then poured into ice-water to produce a white precipitate. The precipitate was filtered and washed several times with water, methanol and dichloromethane. The product was then dried at 60 °C to yield 0.70 g (60% yield) BFTB-4CHO as a red powder. The product was partially soluble in common organic solvent, so we performed H NMR spectroscopy only. ¹H-NMR (500 MHz, DMSO-*d*₆) δ (ppm): 10.10 (s, 4H), 8.65 (s, 4H), 8.43 (d, *J* = 6 Hz, 4H), 8.14 (d, *J* = 6 Hz, 4H), 8.08 (d, *J* = 6 Hz, 4H), 7.78 (d, *J* = 6 Hz, 4H).



Scheme S3. Synthesis of 4,4',4'',4'''-(9,9'-bifluorenylidene)-3,3',6,6'-tetrayl)tetraaniline (BFTB-4NH₂).

4,4',4'',4'''-(9,9'-bifluorenylidene)-3,3',6,6'-tetrayl)tetraaniline (BFTB-4NH₂): A 100 mL round-bottom flask was charged with BF-4Br (1 g, 1.55 mmol), 4-aminophenylboronic acid pinacol ester (2.70 g, 12.3 mmol), tetrakis(triphenylphosphine)palladium(0) 90 mg, 0.077 mmol), and potassium carbonate (2.15 g, 15.55 mmol). The solids were evacuated under high pressure for 15 minutes. Then, dioxane (50 mL) and water (10 mL) were added and the reaction mixture allowed to heat at 100 °C for 48 hours under N₂. After the consumption of BF-4Br, the reaction mixture was cooled to room-temperature and then poured into ice-water to produce a white precipitate. The

precipitate was filtered and washed several times with water, methanol. The product was then dried at 60 °C to yield 0.80 g (74% yield) BFTB-4NH₂ as a blue powder. ¹H-NMR (500 MHz, DMSO-*d*₆) δ (ppm): 8.32 (s, 4H), 8.29 (d, *J* = 12 Hz, 4H), 7.66 (d, *J* = 12 Hz, 8H), 7.53 (d, *J* = 12 Hz, 4H), 6.71 (d, *J* = 12 Hz, 8H), 5.40 (s, br., 8H, 4NH₂). ¹³C NMR (125 MHz, DMSO-*d*₆) δ (ppm): 148.93, 141.30, 141.05, 137.60, 135.53, 127.27, 126.66, 126.24, 123.55, 116.85, 114.10.



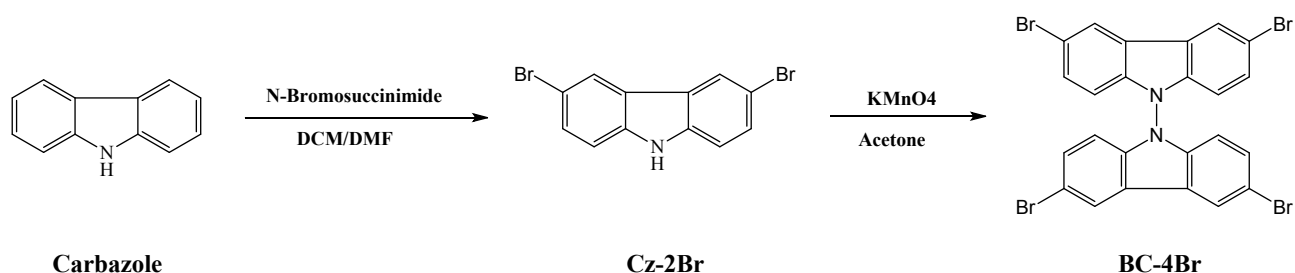
Scheme S4. Synthesis of 4,4',4'',4'''-pyrene-1,3,6,8-tetrayl)tetraaniline (PyTA-4NH₂).

1,3,6,8-tetrabromopyrene (Pyrene-4Br): was prepared as described in the literature with minor modifications.^[S3] A 500 mL round-bottom flask was charged with pyrene (5.0 g, 24 mmol) and nitrobenzene (200 mL) and then bromine (5.6 mL, 109 mmol) was added dropwise through a dropping funnel. The reaction mixture was allowed to reflux at 120 °C for 15 hours. After the consumption of bromine, pale yellow crystallites of 1,3,6,8-tetrabromopyrene were separated from the reaction mixture as precipitate. The suspension was filtrate and the pale-yellow product was washed several times with ethanol and dried under pressure for 12 hours to yield the product in 94%. FTIR: 1592, 1466, 1450, 1228, 1052, 988, 871, 812 cm⁻¹.

4,4',4'',4'''-pyrene-1,3,6,8-tetrayl)tetraaniline (PyTA-4NH₂): A 100 mL round-bottom flask was charged with pyrene-4Br (2.0 g, 3.8 mmol), bis(pinacolato)diboron (5.98 g, 23.56 mmol), [1,1'-Bis(diphenylphosphino)ferrocene]dichloro palladium(II) (241 mg, 0.033 mmol), and potassium acetate (2.33 g, 23.37 mmol). The solids were evacuated under high pressure for 15 minutes. Then, dioxane (40 mL) was added and the reaction mixture allowed to reflux for 48 hours under N₂. After the consumption of pyrene-4Br, the reaction mixture was cooled to room-temperature and then poured into ice-water to produce a yellow precipitate. The precipitate was filtered and washed several times with water and purified using flash column chromatography with THF/hexane as eluent. The isolate solid was finally recrystallized with methanol to give 1,3,6,8-tetrakis(4,4,5,5-tetramethyl-1,3,2-dioxaborolan-2-yl)pyrene (TTDBPy) as yellow crystals (70% yield).

A 100 mL round-bottom flask was charged with TTDBPy (1.0 g, 1.41 mmol), 4-bromoaniline (1.95 g, 11.33 mmol), tetrakis(triphenylphosphine)palladium(0) (80.88 mg, 0.07 mmol), and potassium carbonate (1.95 g, 14.1 mmol). The solids were evacuated under high pressure for 15 minutes. Then, dioxane (40 mL) and water (7 mL) were added and the reaction mixture allowed to heat at 100 °C for 48 hours under N₂. After the consumption of TTDBPy, the reaction mixture was cooled to room-temperature and then poured into ice-water to produce a yellow-greenish precipitate. The precipitate was filtered and washed several times with water, methanol and dichloromethane. The isolate solid of 4,4',4'',4'''-pyrene-1,3,6,8-tetrayl)tetraaniline (Py-TA-4NH₂) was used without further purification (75% yield). ¹H NMR (500 MHz, DMSO) δ (ppm): 8.12 (s, 4H), 7.79 (s, 2H), 7.35 (d, *J* = 12 Hz, 8H), 6.78 (d, *J* = 12 Hz, 8H), 5.30 (s, br., 8H, 4NH₂). ¹³C

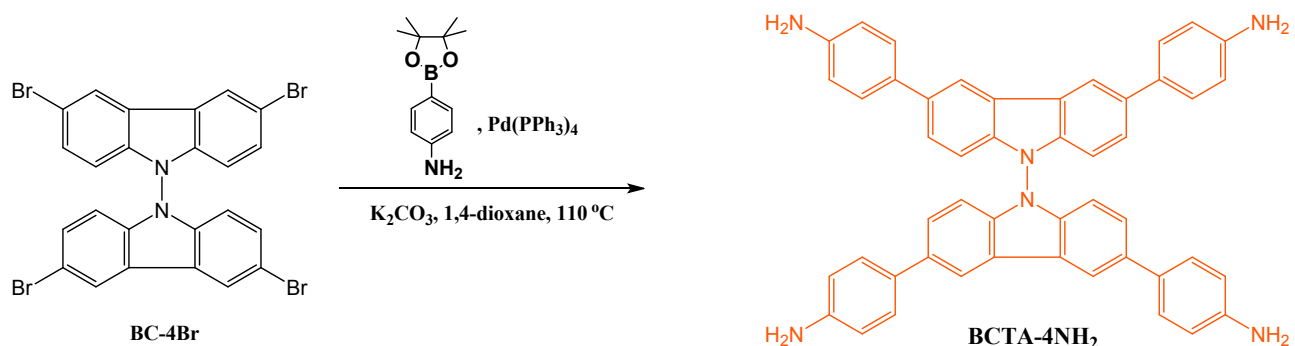
NMR (125 MHz, DMSO) δ (ppm): 148.21, 137.14, 131.06, 129.04, 127.60, 126.72, 126.13, 124.43, 113.96.



Scheme S5. Synthesis of 3,3',6,6'-Tetrabromo-9,9'-bicarbazole (BC-4Br).

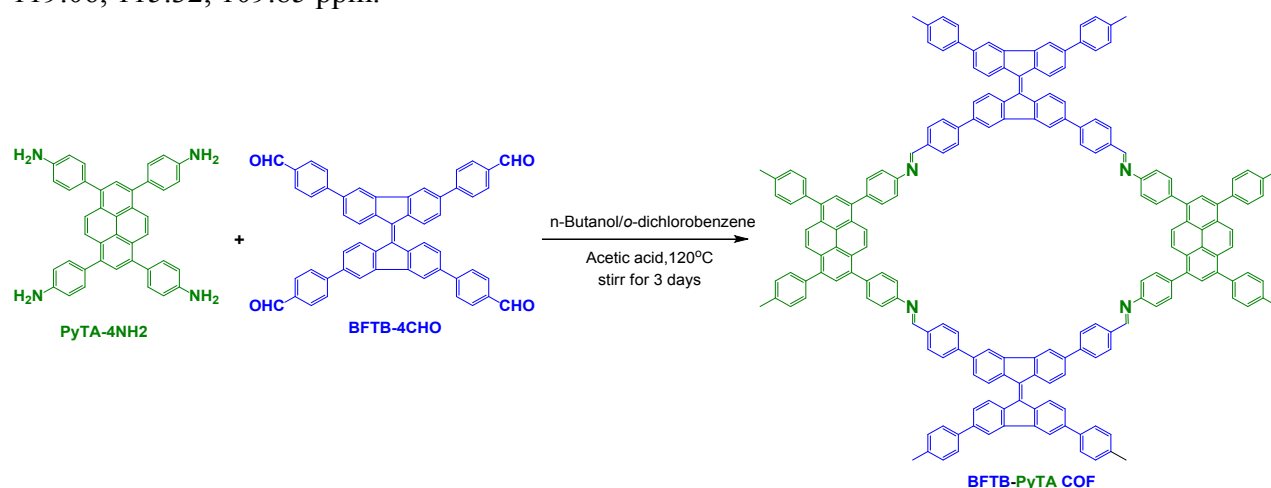
3,6-Dibromo-9H-carbazole (Cz-2Br). Cz-2Br was prepared as previously reported with slight modification. ^[S4] To a suspension of carbazole (5 g, 30 mmol) in dichloromethane (300 mL), a solution of *N*-Bromosuccinimide (NBS) (10.68 g, 60 mmol) in 50 mL DMF was added slowly. The reaction mixture was stirred at room temperature overnight. The solution was washed with water (3 \times 150 mL), then the organic layer was separated, and the solvent was evaporated. The solid was washed with DCM, then collected and dried under vacuum to yield 3,6-dibromocarbazole (7.7 g, yield: 82%) of the product. ¹H NMR (500 MHz, DMSO) δ (ppm): 11.58 (NH, 1H), 8.41 (s, 2H), 7.52 (d, J = 8.5 Hz, 2H), 7.42 (d, J = 2 Hz, 2H). ¹³C NMR (125 MHz, DMSO) δ (ppm): 139.42, 129.42, 124.34, 123.47, 112.97, 112.32.

3,3',6,6'-Tetrabromo-9,9'-bicarbazole (BC-4Br). BC-4Br was prepared as previously reported with slight modification. ^[S4] Potassium permanganate (2.92 g, 90 mmol) was added to a solution of 3,6-dibromocarbazole (2 g, 30 mmol) in 40 mL acetone at 50 °C. Then the solution was hydrolyzed with 100 mL distilled water. The mixture was extracted with dichloromethane and the solvent was evaporated. The residue was washed with methanol to yield 3,3',6,6'-tetrabromo-9,9'-bicarbazole (6.92 g, yield: 71%). ¹H NMR (500 MHz, CDCl₃) δ (ppm): 8.27 (d, 4H), 7.47 (dd, J = 8.5 Hz, 4H), 6.75 (d, J = 8.5 Hz, 4H). ¹³C NMR (125 MHz, CDCl₃) δ (ppm): 139.31, 131.19, 124.81, 123.30, 115.41, 110.59.



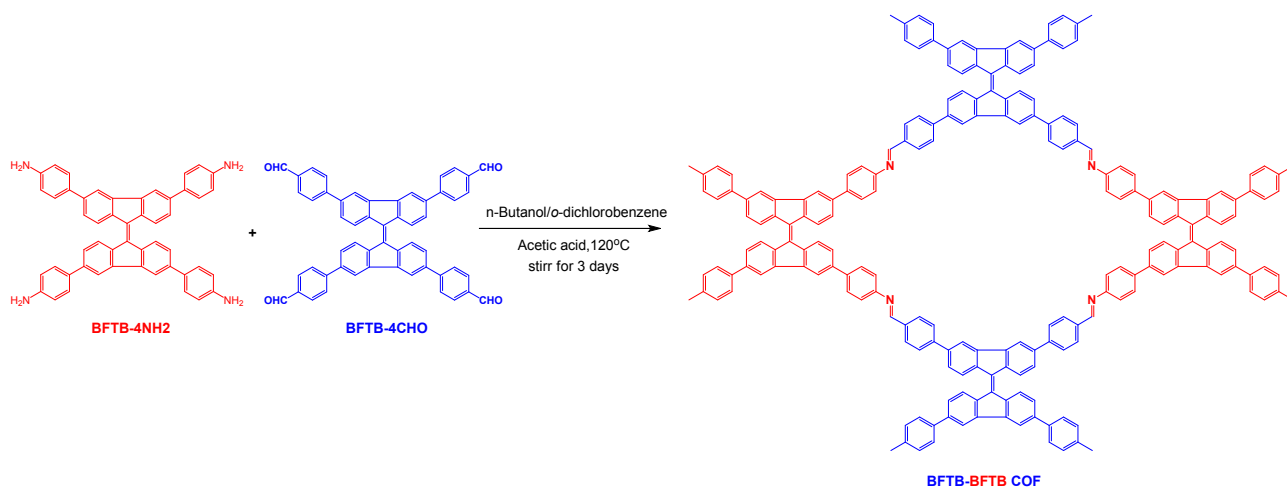
Scheme S6. Synthesis of 4,4',4'',4'''-([9,9'-bicarbazole]-3,3',6,6'-tetrayl)tetraaniline (BCTA-4NH₂).

4,4',4'',4'''-(9,9'-bicarbazole)-3,3',6,6'-tetrayl)tetraaniline (BCTA-4NH₂): Take a pair of two neck flask, add BC-4Br (1 g, 1.54 mmol), 4-aminophenylboronic acid pinacol ester (2.7 g, 12.34 mmol), Pd (PPh₃)₄ (90 mg, 0.078 mmol), K₂CO₃ (2.13 g, 15.41 mmol) in order and vacuum for 15 minutes. Add 50 mL dioxane and 8ml H₂O, then heat to 100 °C in an oil pot and the mixture was stirred at 100 °C for 48 h. Pour the solution into a beaker filled with ice cubes and H₂O and stir, then suction filter. The crude product was purified over a chromatographic silica gel column (hexane/AcOEt, 3:1) to give the pure BCTA-4NH₂. FTIR (powder): ¹H-NMR (DMSO-d₆, 25 °C, 500 MHz): δ= 8.63 (s, 4H), 7.56 (s, 4H), 7.50 (s, 8H), 6.86 (s, 4H), 6.70 (d, *J* = 10 Hz, 8H), 5.18 (s, 8H). ¹³C-NMR (DMSO-*d*₆, 25 °C, 125 MHz): 149.14, 139.72, 135.8, 129.3, 128.52, 125.95, 123.63, 119.06, 115.32, 109.85 ppm.



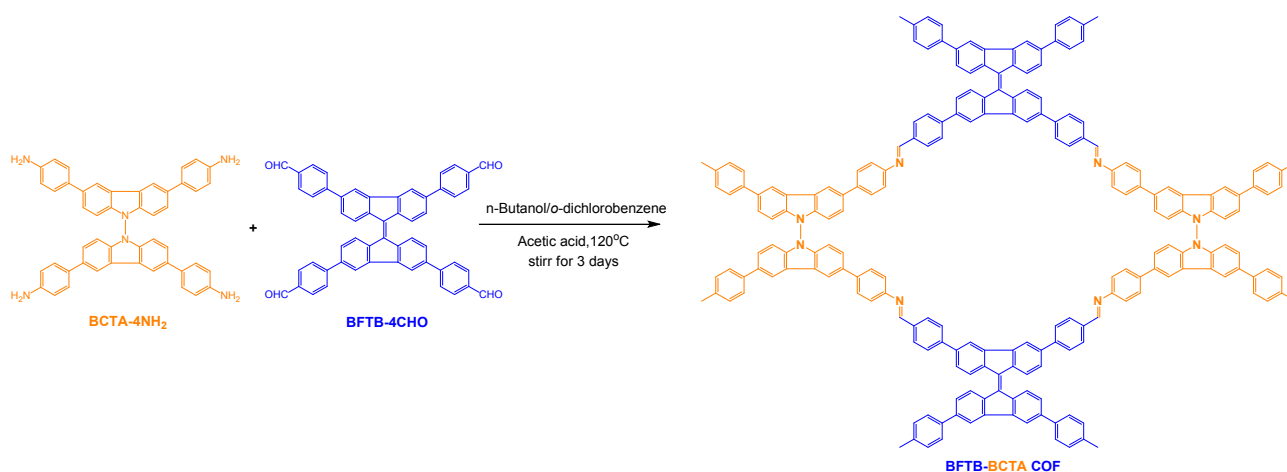
Scheme S7. Synthesis of BFTB-PyTA COF.

In a 25-mL Schlenk storage tube, PyTA-4NH₂ (53 mg, 0.094 mmol) and BFTB-4CHO (70 mg, 0.14 0.094 mmol) was dissolved in n-butanol (3.5 mL) and *o*-dichlorobenzene (3.5 mL) in the presence of acetic acid (6 M, 0.7 mL). The tube was sealed and degassed through three freeze-pump-thaw cycles. The tube was sealed off by flame and heated at 120 °C for 3 days. After cooling to room temperature, the tube was opened and the precipitate filtered and washed two times with n-butanol, THF, and acetone respectively. The solid was dried under vacuum at 120 °C overnight to afford BFTB-PyTA COF as a red powder, (90% yield).



Scheme S8. Synthesis of BFTB-BFTB COF.

In a 25-mL Schlenk storage tube, BFTB-4NH₂ (65 mg, 0.094 mmol) and BFTB-4CHO (70 mg, 0.14 0.094 mmol) was dissolved in n-butanol (3.5 mL) and *o*-dichlorobenzene (3.5 mL) in the presence of acetic acid (6 M, 0.7 mL). The tube was sealed and degassed through three freeze-pump-thaw cycles. The tube was sealed off by flame and heated at 120 °C for 3 days. After cooling to room temperature, the tube was opened and the precipitate filtered and washed two times with n-butanol, THF, and acetone respectively. The solid was dried under vacuum at 120 °C overnight to afford BFTB-BFTB COF as a red powder, (91% yield).



Scheme S9. Synthesis of BFTB-BCTA COF.

In a 25-mL Schlenk storage tube, BCTB-4NH₂ (38 mg, 0.055 mmol) and BFTB-4CHO (40 mg, 0.055 mmol) was dissolved in n-butanol (2 mL) and *o*-dichlorobenzene (2 mL) in the presence of acetic acid (6 M, 0.4 mL). The tube was sealed and degassed through three freeze-pump-thaw

cycles. The tube was sealed off by flame and heated at 120 °C for 3 days. After cooling to room temperature, the tube was opened and the precipitate filtered and washed two times with n-butanol, THF, and acetone respectively. The solid was dried under vacuum at 120 °C overnight to afford BFTB-BCTA COF as a red powder. (91% yield).

S4. FTIR Spectral Profiles of COFs

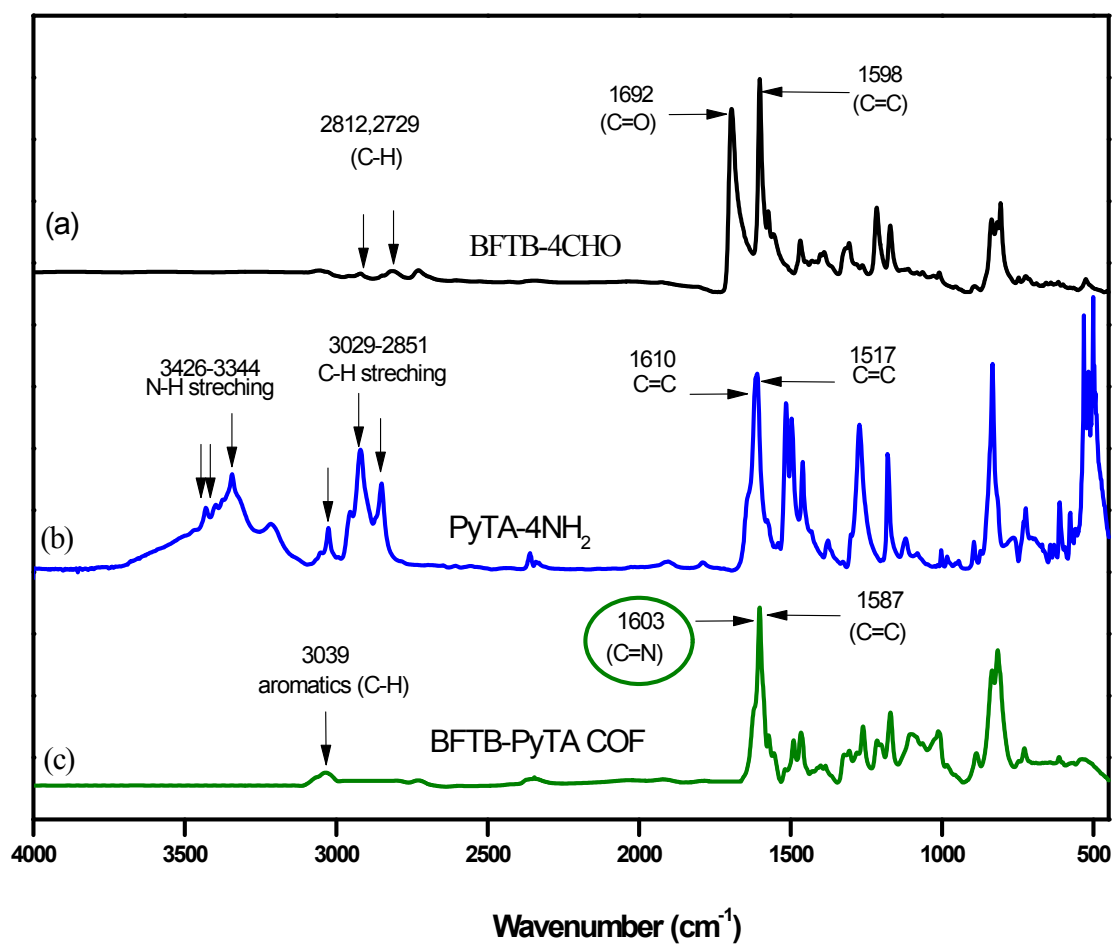


Figure S1. FT-IR spectra of (a) BFTB-4CHO, (b) PyTA-4NH₂, and (c) BFTB-PyTA COF.

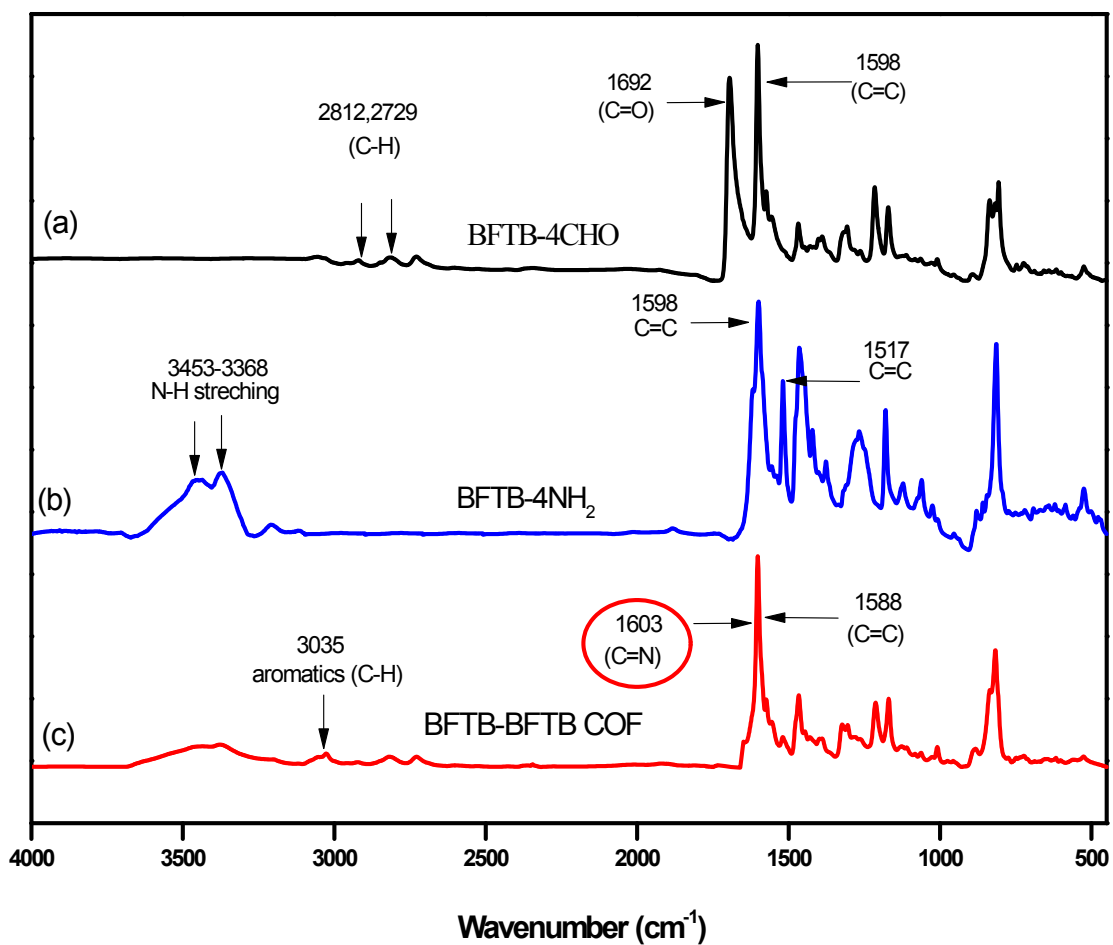


Figure S2. FT-IR spectra of (a) BFTB-4CHO, (b) BFTB-4NH₂, and (c) BFTB-BFTB COF.

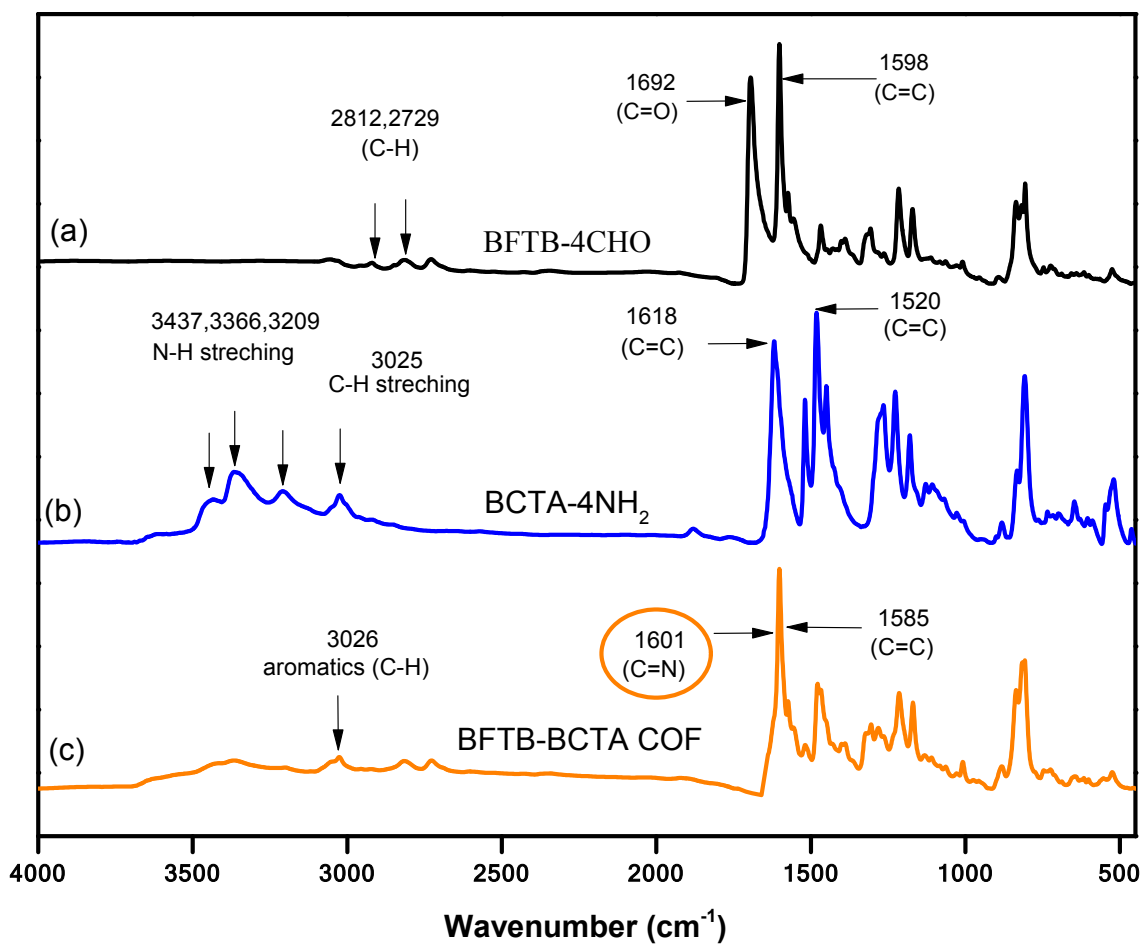


Figure S3. FT-IR spectra of (a) BFTB-4CHO, (b) BCTA-4NH₂, and (c) BFTB- BCTA COF.

S5. Thermal Gravimetric Analysis

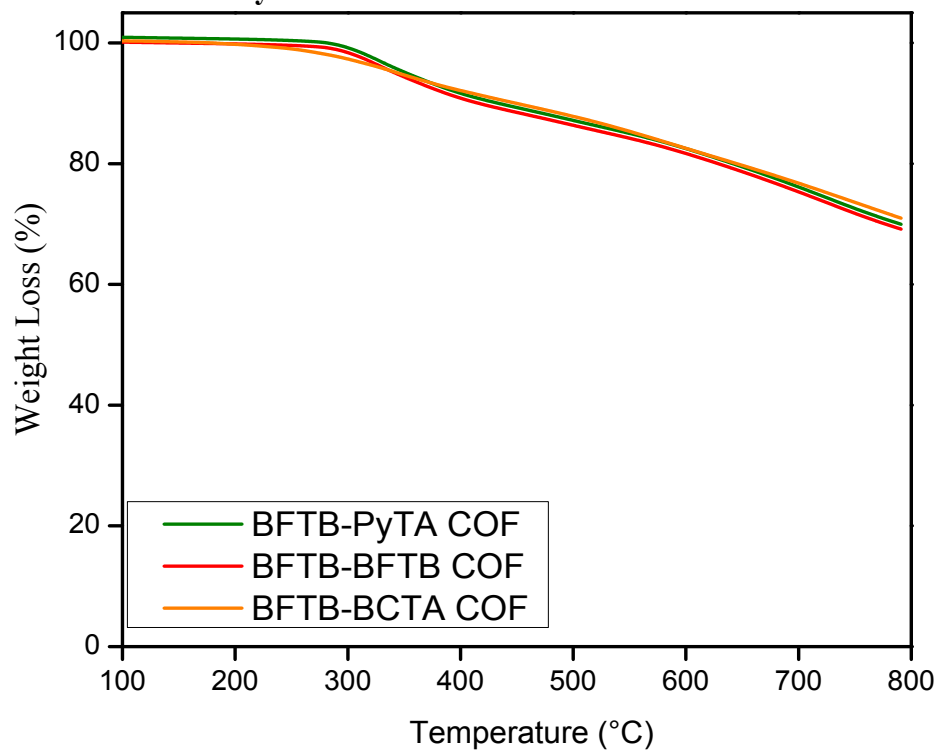


Figure S4. Thermogravimetric analysis trace of BFTB-PyTA, BFTB- BFTB, and BFTB- BCTA COFs under nitrogen atmosphere with heating rate of 20°C min⁻¹.

Table S1. Values of $T_{d10\%}$ and Char yield of COFs.

	$T_{d10\%}$ (°C)	Char yield (%)
BFTB-PyTA COF	433	70
BFTB-BFTB COF	416	69
BFTB-BCTA COF	449	71

S6. Field Emission Scanning Electron Microscopy (FE-SEM)

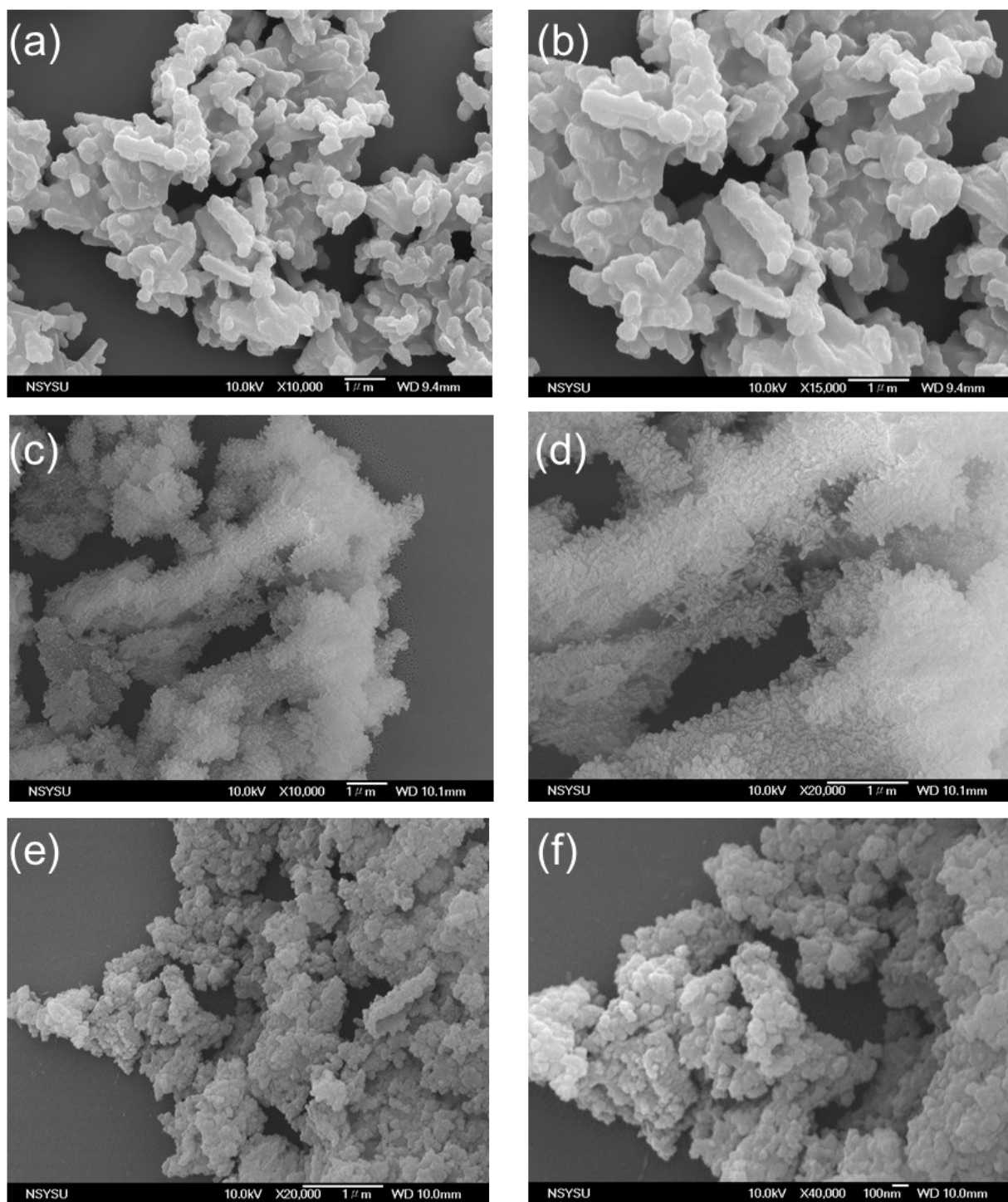


Figure S5. FE-SEM images of (a,b) BFTB-PyTA, (c,d) BFTB-BFTB, and (e,f) BFTB-BCTA COFs at different magnification scales.

S7. Transmission Electron Microscopy (TEM)

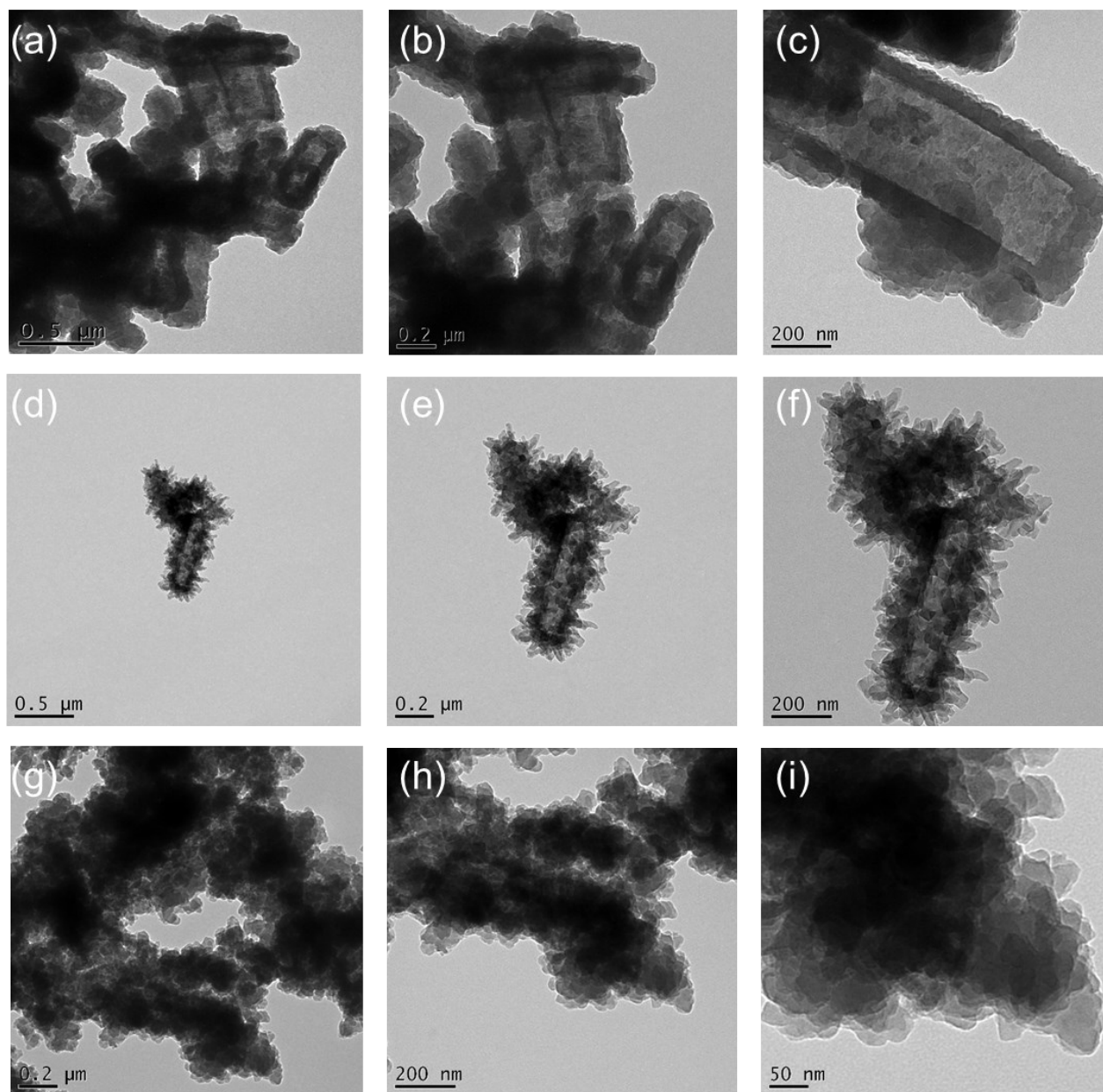


Figure S6. TEM images of (a-c) BFTB-PyTA, (d-f) BFTB-BFTB, and (g-i) BFTB-BCTA COFs at different magnification scales.

S8. Experimental and Simulation X-ray Diffraction Patterns for COFs Structures

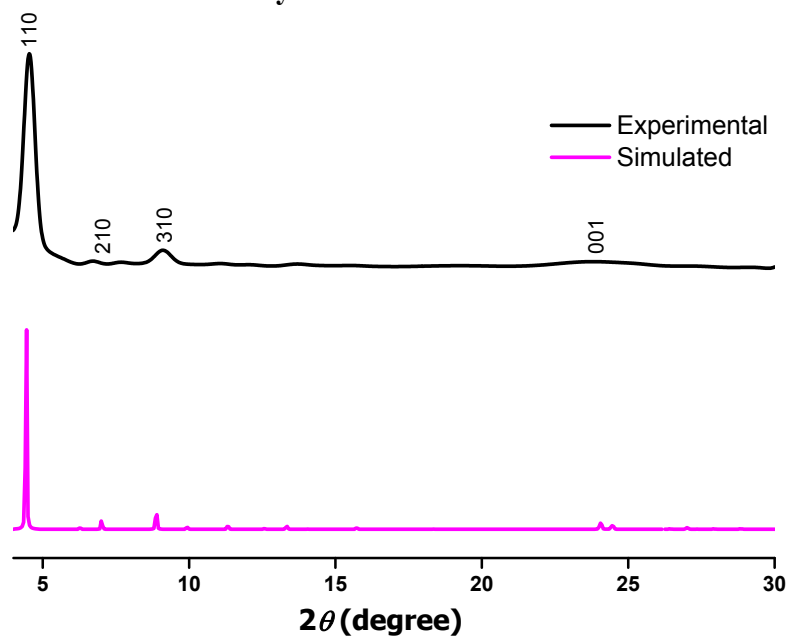


Figure S7. PXRD pattern of the as-synthesized BFTB-PyTA COF (black), compared with the simulated PXRD pattern of the eclipsed AA-stacking model (purple).

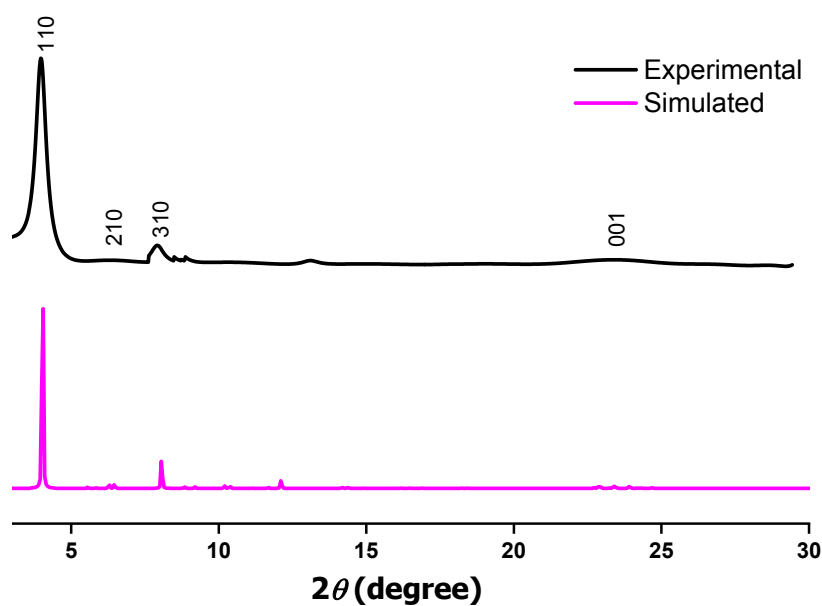


Figure S8. PXRD pattern of the as-synthesized BFTB-BFTB COF (black), compared with the simulated PXRD pattern of the eclipsed AA-stacking model (purple).

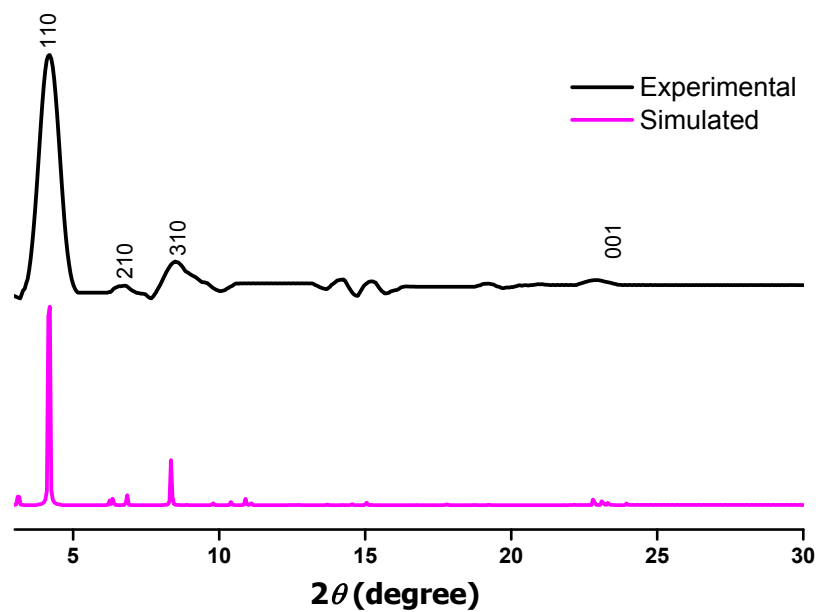


Figure S9. PXRD pattern of the as-synthesized BFTB-BCTA COF (black), compared with the simulated PXRD pattern of the eclipsed AA-stacking model (purple).

S9. PXRD data and BET parameters

Table S2. PXRD and BET parameters of the synthesized COFs.

COF	S_{BET} ($\text{m}^2 \text{g}^{-1}$)	d_{110} (nm)	Pore size (nm)	Pore volume ($\text{cm}^3 \text{g}^{-1}$)	Interlayer Distance (\AA)
BFTB-PyTA	1133	1.94	1.63	0.41	3.71
BFTB-BFTB	1040	2.19	1.78, 1.11	0.69	3.79
BFTB-BCTA	834	2.11	1.75, 1.07	0.67	3.87

S10. Structural Modeling and Fractional atomic coordinates for COF Structures

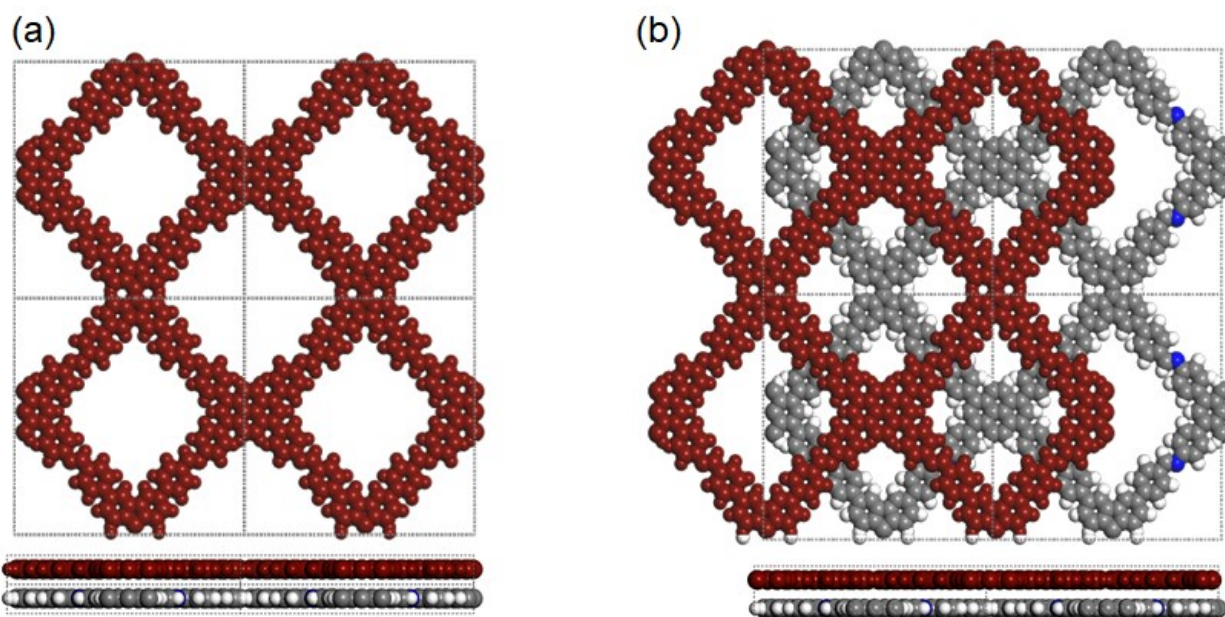


Figure S10. Crystalline structure for BFTB-PyTA COF based on (a) AA-eclipsed stacking models (b) AB-staggered stacking models.

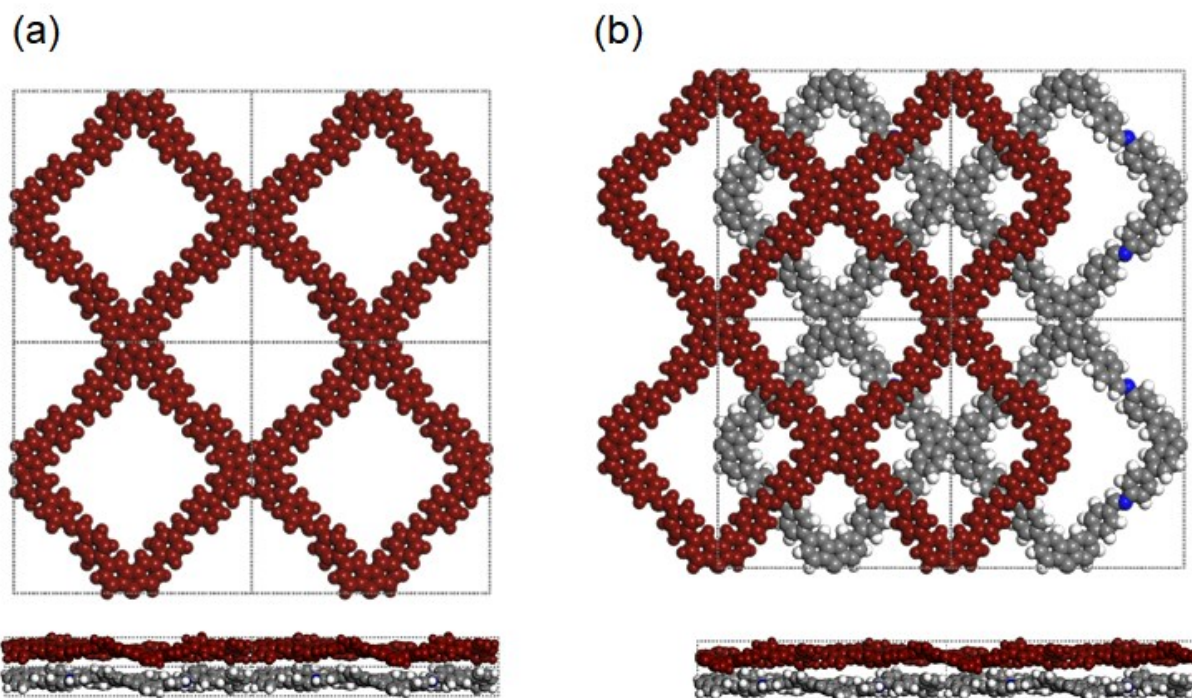


Figure S11. Crystalline structure for BFTB-BFTB COF based on (a) AA-eclipsed stacking models (b) AB-staggered stacking models.

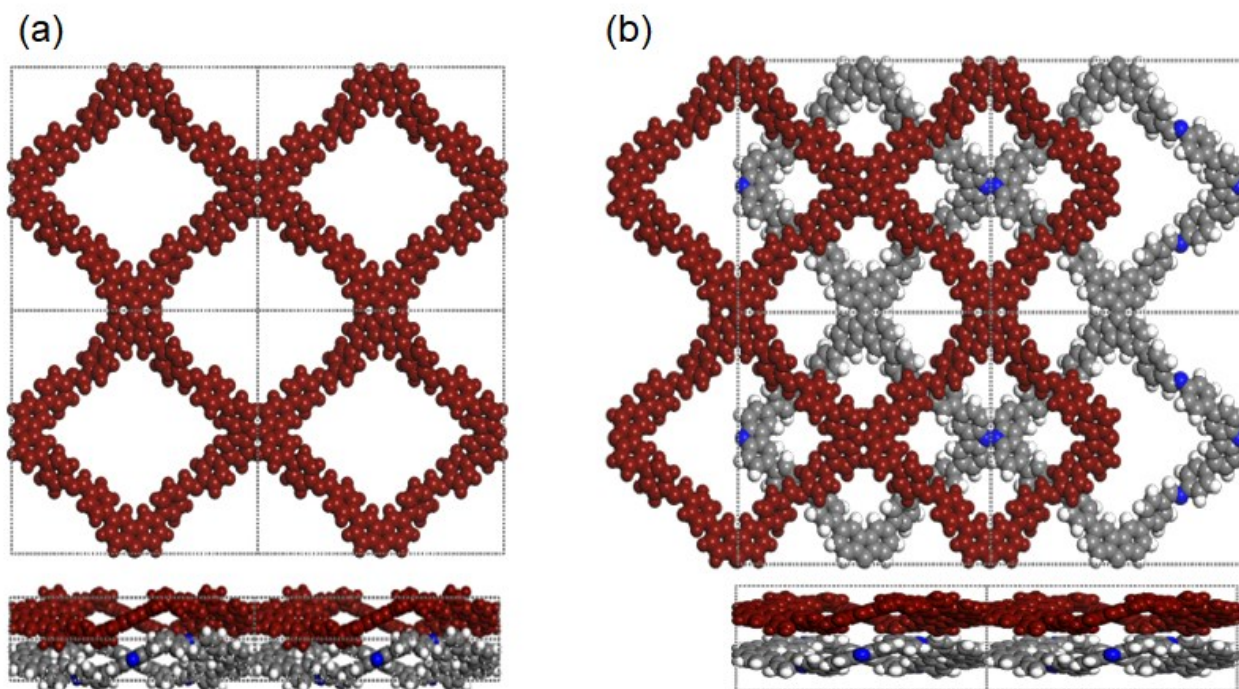


Figure S12. Crystalline structure for BFTB-BCTA COF based on (a) AA-eclipsed stacking models (b) AB-staggered stacking models.

Table S3. Fractional atomic coordinates for the unit cell of BFTB-PyTA COF with AA-stacking.

Sample Name : BFTB-PyTA COF							
Space Group : P 1							
a = 24.918, b = 31.042, c = 3.528				$\alpha = \beta = \gamma = 90^\circ$			
R _{wp} = 8.70%				R _p = 6.12%			
Atom	x/a	y/b	z/c	Atom	x/a	y/b	z/c
C1	0.49862	0.91631	0.51787	C30	0.00055	0.43426	0.51787
C2	0.54956	0.91631	0.51787	C31	0.04873	0.43426	0.51787
C3	0.56557	0.96263	0.51787	C32	0.07461	0.47652	0.51787
C4	0.52409	0.99586	0.51787	C33	0.12499	0.47643	0.51787
C5	0.48262	0.96263	0.51787	C34	0.14831	0.52016	0.51787
C6	0.43377	0.97109	0.51786	C35	0.12499	0.56389	0.51787
C7	0.40199	0.93269	0.51787	C36	0.15571	0.60742	0.51787
C8	0.41886	0.88556	0.51787	C37	0.15571	0.4329	0.51787
C9	0.46812	0.87752	0.51787	C38	0.20541	0.60226	0.51787
C10	0.58007	0.87752	0.51787	C39	0.2353	0.64165	0.51787
C11	0.62933	0.88556	0.51787	C40	0.21624	0.68759	0.51787
C12	0.64619	0.93269	0.51787	C41	0.16694	0.69334	0.51787
C13	0.61442	0.97109	0.51787	C42	0.13708	0.65368	0.51787
C14	0.38558	0.84489	0.51787	C43	0.13708	0.38665	0.51787
C15	0.66261	0.84489	0.51787	C44	0.16694	0.34698	0.51787
C16	0.33618	0.85195	0.51787	C45	0.21624	0.35273	0.51786
C17	0.30514	0.81317	0.51787	C46	0.2353	0.39867	0.51786
C18	0.32325	0.76686	0.51787	C47	0.20541	0.43807	0.51787
C19	0.37229	0.75967	0.51787	C48	0.54956	0.12401	0.51787
C20	0.4032	0.79832	0.51787	C49	0.49862	0.12401	0.51787
C21	0.64498	0.79832	0.51787	C50	0.48262	0.07769	0.51787
C22	0.67589	0.75967	0.51787	C51	0.52409	0.04446	0.51787
C23	0.72493	0.76686	0.51787	C52	0.56557	0.07769	0.51787
C24	0.74304	0.81317	0.51787	C53	0.61442	0.06923	0.51787
C25	0.71201	0.85195	0.51787	C54	0.64619	0.10763	0.51787
C26	0.04941	0.52016	0.51787	C55	0.62933	0.15476	0.51787
C27	0.07461	0.56381	0.51787	C56	0.58007	0.16281	0.51787
C28	0.04873	0.60606	0.51787	C57	0.46812	0.16281	0.51787
C29	0.00055	0.60606	0.51787	C58	0.41886	0.15476	0.51787

Continuous (Table S3)

Atom	x/a	y/b	z/c	Atom	x/a	y/b	z/c
C59	0.41886	0.15476	0.51787	C94	0.29221	0.3151	0.51787
C60	0.40199	0.10763	0.51787	N95	0.24629	0.72861	0.51787
C61	0.43377	0.06923	0.51787	N96	0.24629	0.31171	0.51786
C62	0.66261	0.19544	0.51787	N97	0.33618	0.18838	0.51787
C63	0.38558	0.19544	0.51787	N98	0.8019	0.31171	0.51787
C64	0.71201	0.18838	0.51787	H99	0.41981	1.00904	0.51786
C65	0.74304	0.22715	0.51787	H100	0.36206	0.93941	0.51787
C66	0.72493	0.27346	0.51786	H101	0.48244	0.83969	0.51787
C67	0.67589	0.28065	0.51787	H102	0.56499	0.83999	0.51786
C68	0.64498	0.24201	0.51787	H103	0.68603	0.93995	0.51787
C69	0.4032	0.24201	0.51787	H104	0.62855	1.00898	0.51787
C70	0.37229	0.28065	0.51787	H105	0.3211	0.88948	0.51787
C71	0.32325	0.27346	0.51787	H106	0.26511	0.81923	0.51787
C72	0.30514	0.22715	0.51787	H107	0.38723	0.72208	0.51787
C73	0.8019	0.72861	0.51787	H108	0.44324	0.79226	0.51787
C74	0.84278	0.43807	0.51787	H109	0.60502	0.79178	0.51787
C75	0.81288	0.39867	0.51787	H110	0.66112	0.72202	0.51787
C76	0.83195	0.35273	0.51787	H111	0.78307	0.81926	0.51787
C77	0.88124	0.34698	0.51787	H112	0.72677	0.8896	0.51786
C78	0.9111	0.65368	0.51787	H113	0.06809	0.64158	0.51787
C79	0.88124	0.69334	0.51787	H114	0.02079	0.64108	0.51786
C80	0.83195	0.68759	0.51787	H115	0.02079	0.39925	0.51786
C81	0.81288	0.64165	0.51787	H116	0.06898	0.39925	0.51787
C82	0.84278	0.60226	0.51787	H117	0.18878	0.52154	0.51787
C83	0.89247	0.4329	0.51787	H118	0.22192	0.56533	0.51787
C84	0.89247	0.60742	0.51787	H119	0.27548	0.63661	0.51787
C85	0.9232	0.56389	0.51787	H120	0.15091	0.73047	0.51787
C86	0.89987	0.52016	0.51787	H121	0.09688	0.65855	0.51787
C87	0.9232	0.47643	0.51787	H122	0.09699	0.38095	0.51787
C88	0.97357	0.47652	0.51787	H123	0.15108	0.30978	0.51787
C89	0.97357	0.56381	0.51787	H124	0.27545	0.40395	0.51786
C90	0.99877	0.52016	0.51787	H125	0.22113	0.47533	0.51787
C91	0.75598	0.72522	0.51787	H126	0.62837	0.03128	0.51787
C92	0.75598	0.3151	0.51786	H127	0.68612	0.10091	0.51787
C93	0.29221	0.72522	0.51786	H128	0.56575	0.20063	0.51787

Continuous (Table S3)

Atom	x/a	y/b	z/c	Atom	x/a	y/b	z/c
H129	0.4832	0.20033	0.51787				
H130	0.36216	0.10037	0.51787				
H131	0.41963	0.03134	0.51787				
H132	0.72708	0.15085	0.51787				
H133	0.78308	0.22109	0.51787				
H134	0.66096	0.31824	0.51786				
H135	0.60494	0.24806	0.51787				
H136	0.44317	0.24854	0.51787				
H137	0.38706	0.3183	0.51787				
H138	0.26511	0.22106	0.51787				
H139	0.32142	0.15072	0.51787				
H140	0.82627	0.47499	0.51786				
H141	0.7727	0.40371	0.51787				
H142	0.89728	0.30985	0.51787				
H143	0.9513	0.38177	0.51787				
H144	0.9512	0.65937	0.51787				
H145	0.89711	0.73055	0.51787				
H146	0.77273	0.63638	0.51787				
H147	0.82705	0.56499	0.51787				
H148	0.8594	0.51878	0.51787				
H149	0.73993	0.68809	0.51787				
H150	0.73993	0.35223	0.51786				
H151	0.30825	0.68809	0.51786				
H152	0.30825	0.35223	0.51787				

Table S4. Fractional atomic coordinates for the unit cell of BFTB-BFTB COF with AA-stacking.

Sample Name: BFTB-BFTB COF							
Space Group: P 1							
a = 24.664, b = 31.454, c = 3.291 $\alpha = \beta = \gamma = 90^\circ$							
R _{wp} = 7.69%				R _p = 6.09%			
Atom	x/a	y/b	z/c	Atom	x/a	y/b	z/c
C1	0.4817	0.90038	0.59817	C29	0.47147	0.0823	0.68205
C2	0.52902	0.90244	0.66519	C30	0.45678	0.0405	0.67104
C3	0.5431	0.94435	0.66394	C31	0.4983	0.01393	0.59733
C4	0.50209	0.97115	0.59388	C32	0.53384	0.04489	0.54378
C5	0.46634	0.94021	0.53419	C33	0.57416	0.0399	0.37364
C6	0.42644	0.94528	0.35501	C34	0.60311	0.07478	0.34562
C7	0.39785	0.91003	0.31267	C35	0.59	0.11532	0.4672
C8	0.41125	0.86927	0.42816	C36	0.54634	0.12013	0.59326
C9	0.45483	0.86467	0.56168	C37	0.44271	0.11639	0.71584
C10	0.55809	0.86849	0.68861	C38	0.39697	0.10963	0.759
C11	0.60368	0.8759	0.73402	C39	0.38166	0.06744	0.77294
C12	0.61863	0.91799	0.7625	C40	0.4102	0.03248	0.72941
C13	0.58935	0.95271	0.72622	C41	0.62004	0.15291	0.44627
C14	0.38094	0.8318	0.4047	C42	0.3661	0.14676	0.78278
C15	0.63494	0.83936	0.73191	C43	0.66553	0.14966	0.52706
C16	0.33516	0.83564	0.4701	C44	0.6927	0.1856	0.53578
C17	0.30754	0.79991	0.48049	C45	0.67544	0.22575	0.45726
C18	0.32494	0.75931	0.42123	C46	0.63041	0.22862	0.36596
C19	0.37034	0.7556	0.34924	C47	0.60332	0.1928	0.35639
C20	0.39787	0.79108	0.33938	C48	0.38195	0.1863	0.90272
C21	0.62226	0.8	0.87668	C49	0.356	0.22251	0.8774
C22	0.64868	0.76424	0.83148	C50	0.31234	0.22028	0.74733
C23	0.68911	0.76667	0.64837	C51	0.29553	0.18077	0.6416
C24	0.70279	0.80599	0.51773	C52	0.32203	0.1445	0.65903
C25	0.67602	0.84198	0.55855	C53	0.09487	0.47022	0.53114
C26	0.29663	0.72061	0.43247	C54	0.09535	0.51622	0.54856
C27	0.28672	0.25983	0.70592	C55	0.05169	0.53017	0.56254
C28	0.51877	0.08467	0.61697	C56	0.02007	0.49353	0.53304

Continuous (Table S4)

Atom	x/a	y/b	z/c	Atom	x/a	y/b	z/c
C57	0.05105	0.45665	0.50906	C92	0.94897	0.42134	0.781
C58	0.0427	0.41423	0.43332	C93	0.84416	0.62384	0.34288
C59	0.07735	0.38532	0.43718	C94	0.83702	0.36731	0.64548
C60	0.12107	0.39769	0.51268	C95	0.85964	0.66485	0.41395
C61	0.13027	0.44131	0.54194	C96	0.83043	0.6986	0.45389
C62	0.13148	0.54441	0.54479	C97	0.78474	0.69256	0.4351
C63	0.1233	0.58844	0.57463	C98	0.76869	0.65174	0.36462
C64	0.07921	0.60142	0.64191	C99	0.7981	0.61772	0.32136
C65	0.044	0.57292	0.63536	C100	0.7911	0.37503	0.66356
C66	0.15528	0.36404	0.57232	C101	0.76033	0.34178	0.63108
C67	0.15895	0.6216	0.53401	C102	0.77458	0.29991	0.5796
C68	0.14215	0.32523	0.72625	C103	0.82019	0.29216	0.55792
C69	0.17179	0.29166	0.75606	C104	0.85082	0.32513	0.5864
C70	0.2158	0.29606	0.64943	N105	0.24358	0.2595	0.67553
C71	0.22984	0.33484	0.50526	N106	0.25381	0.72275	0.46603
C72	0.19987	0.36865	0.46723	N107	0.75627	0.7287	0.48423
C73	0.20338	0.61449	0.63145	N108	0.74464	0.26432	0.55764
C74	0.23518	0.6471	0.60771	H109	0.4186	0.97611	0.24586
C75	0.22321	0.68765	0.48204	H110	0.36664	0.91451	0.176
C76	0.17915	0.69453	0.38633	H111	0.46718	0.83423	0.64201
C77	0.14801	0.66204	0.40271	H112	0.5454	0.83686	0.6564
C78	0.7028	0.26509	0.47495	H113	0.65341	0.92421	0.81655
C79	0.71546	0.72774	0.59811	H114	0.60658	0.98385	0.76751
C80	0.90018	0.51647	0.44513	H115	0.32077	0.86613	0.52521
C81	0.89881	0.47235	0.5497	H116	0.27272	0.80366	0.53844
C82	0.94202	0.45967	0.61191	H117	0.38443	0.72485	0.30064
C83	0.97435	0.49377	0.52231	H118	0.43256	0.78667	0.27898
C84	0.94403	0.52825	0.40775	H119	0.59196	0.79719	1.0311
C85	0.95376	0.5663	0.2458	H120	0.63774	0.73464	0.94528
C86	0.92047	0.59624	0.1999	H121	0.73384	0.80863	0.37622
C87	0.8765	0.58806	0.31246	H122	0.68663	0.87134	0.44103
C88	0.86581	0.54611	0.41449	H123	0.31244	0.69026	0.39276
C89	0.8631	0.44392	0.56591	H124	0.3041	0.28983	0.73116
C90	0.87116	0.40178	0.67739	H125	0.58245	0.0094	0.26126
C91	0.91405	0.39227	0.8097	H126	0.63452	0.07045	0.21669

Continuous (Table S4)

H127	0.53346	0.15059	0.66837	H163	0.73359	0.64624	0.33671
H128	0.45612	0.14796	0.69321	H164	0.78463	0.587	0.26857
H129	0.34722	0.06115	0.81442	H165	0.77901	0.40661	0.71084
H130	0.39212	0.00132	0.74058	H166	0.72569	0.34881	0.65517
H131	0.6795	0.11938	0.59662	H167	0.83206	0.26029	0.51082
H132	0.72705	0.18229	0.61039	H168	0.88563	0.31732	0.55087
H133	0.61628	0.25915	0.30198				
H134	0.56905	0.19643	0.27979				
H135	0.41451	0.18952	1.01514				
H136	0.36991	0.25224	0.96365				
H137	0.26199	0.17838	0.53429				
H138	0.30837	0.11502	0.56079				
H139	0.01018	0.40186	0.37651				
H140	0.06938	0.35289	0.3861				
H141	0.16352	0.45211	0.58794				
H142	0.16464	0.53256	0.51203				
H143	0.07151	0.63416	0.6954				
H144	0.01133	0.58538	0.67976				
H145	0.10883	0.32088	0.82792				
H146	0.16086	0.2622	0.87285				
H147	0.26305	0.33846	0.40494				
H148	0.211	0.3974	0.34077				
H149	0.21319	0.58428	0.73895				
H150	0.2685	0.64118	0.69928				
H151	0.1694	0.72512	0.28721				
H152	0.11504	0.66864	0.3093				
H153	0.68694	0.2945	0.40803				
H154	0.70078	0.698	0.67275				
H155	0.98707	0.57316	0.16822				
H156	0.92953	0.62626	0.08139				
H157	0.83254	0.53741	0.48742				
H158	0.83107	0.45395	0.47169				
H159	0.92067	0.36213	0.93634				
H160	0.98114	0.41435	0.88524				
H161	0.89447	0.6712	0.44733				
H162	0.84316	0.73002	0.5045				

Table S5. Fractional atomic coordinates for the unit cell of BFTB-BCTA COF with AA-stacking.

Sample Name: BFTB-BCTA COF							
Space Group: P 2 2 2							
a = 31.909, b = 28.274, c = 4.073 $\alpha=\beta=\gamma=90^\circ$							
R _{wp} = 5.82%				R _p = 4.32%			
Atom	x/a	y/b	z/c	Atom	x/a	y/b	z/c
C1	0.4782	0.89691	0.4509	H30	0.36647	0.92309	0.14984
C2	0.53531	0.9432	0.57575	H31	0.46553	0.82325	0.38283
C3	0.42502	0.95225	0.29495	H32	0.34053	0.86489	0.13417
C4	0.3979	0.91449	0.22772	H33	0.28831	0.80253	0.17692
C5	0.41115	0.86689	0.2644	H34	0.36325	0.71273	0.44166
C6	0.45273	0.85852	0.36943	H35	0.41362	0.77603	0.51659
C7	0.38155	0.82667	0.20129	H36	0.29727	0.6809	0.20463
C8	0.34574	0.83266	0.00219	H37	0.1742	0.74701	0.26064
C9	0.31592	0.79669	0.02749	H38	0.11561	0.69178	0.34041
C10	0.32178	0.75324	0.13142	H39	0.19155	0.57867	0.05205
C11	0.35837	0.74587	0.31382	H40	0.25016	0.63417	0.11907
C12	0.38758	0.78228	0.35279	H41	0.06446	0.64425	0.07522
C13	0.28925	0.71625	0.12291	H42	0.00795	0.59087	0.24475
C14	0.21634	0.69439	0.07324	H43	0.1558	0.54053	0.39398
C15	0.17771	0.71036	0.18956				
C16	0.14441	0.67886	0.23242				
C17	0.14905	0.63076	0.15192				
C18	0.18743	0.61522	0.02015				
C19	0.22088	0.64677	0.01802				
C20	0.1147	0.59676	0.22132				
C21	0.07227	0.61	0.1771				
C22	0.03958	0.57927	0.26653				
C23	0.04907	0.53503	0.39677				
C24	0.09053	0.52215	0.43382				
C25	0.12386	0.55166	0.35021				
C26	0.5	0.9759	0.5				
N27	0.25055	0.27284	0.94092				
N28	0.02248	0.5	0.5				
H29	0.41459	0.9876	0.24765				

S11. Organic Pollutant Treatment in Water

Dye adsorption experiments

The organic dye RhB was selected to study the efficiency of the BFTB-PyTA, BFTB-BFTB, and BFTB-BCTA COFs for the removal of dyes from water. In a typical experiment, a BFTB-PyTA, BFTB-BFTB, or BFTB-BCTA COF (4 mg) was added to an aqueous solution of RhB (10 mL) in a glass vial and then the mixture was stirred (for 0, 5, 10, 15, 20, or 30 min) at a rate of 500 rpm. The supernatant was then isolated through centrifugation (6000 rpm, 10 min). The UV–Vis spectrum of the isolated supernatant was measured. To obtain adsorption isothermal curves, various concentrations of the aqueous dye (from 25 to 200 mg L⁻¹) were used. For each test, a FTB-PyTA, BFTB-BFTB, or BFTB-BCTA COF (2 mg) was added to an aqueous solution of RhB (10 mL) in a glass vial and then the mixture was stirred (500 rpm) for 24 h. The supernatant was isolated through centrifugation and its UV–Vis spectrum recorded, to construct the isothermal curve. Adsorption reusability tests were performed by adding a BFTB-PyTA, BFTB-BFTB, or BFTB-BCTA COF (3 mg) to an aqueous solution of the dye (25 mg L⁻¹, 10 mL) and then stirring for 1 h. The supernatant was isolated and its UV–Vis spectrum recorded. The BFTB-PyTA, BFTB-BFTB, and BFTB-BCTA COFs were washed several times with H₂O, EtOH, THF, and acetone to remove the adsorbed dye. After drying the BFTB-PyTA, BFTB-BFTB, and BFTB-BCTA COFs overnight at 100 °C, they were used in the next dye removal test. The adsorption isothermals of RhB was fitted using the Langmuir isothermal model (linear form), expressed as follows:

$$\frac{C_e}{Q_e} = \frac{1}{K_L Q_m} + \frac{C_e}{Q_m}$$

where C_e (mg L⁻¹) is the equilibrium dye concentration in the liquid phase; Q_e (mg g⁻¹) is the equilibrium adsorption of dye per unit mass of the adsorbent carbon; Q_m (mg g⁻¹) is the maximum equilibrium adsorption of dye per unit mass of the adsorbent carbon; and K_L (L mg⁻¹) is the Langmuir constant.

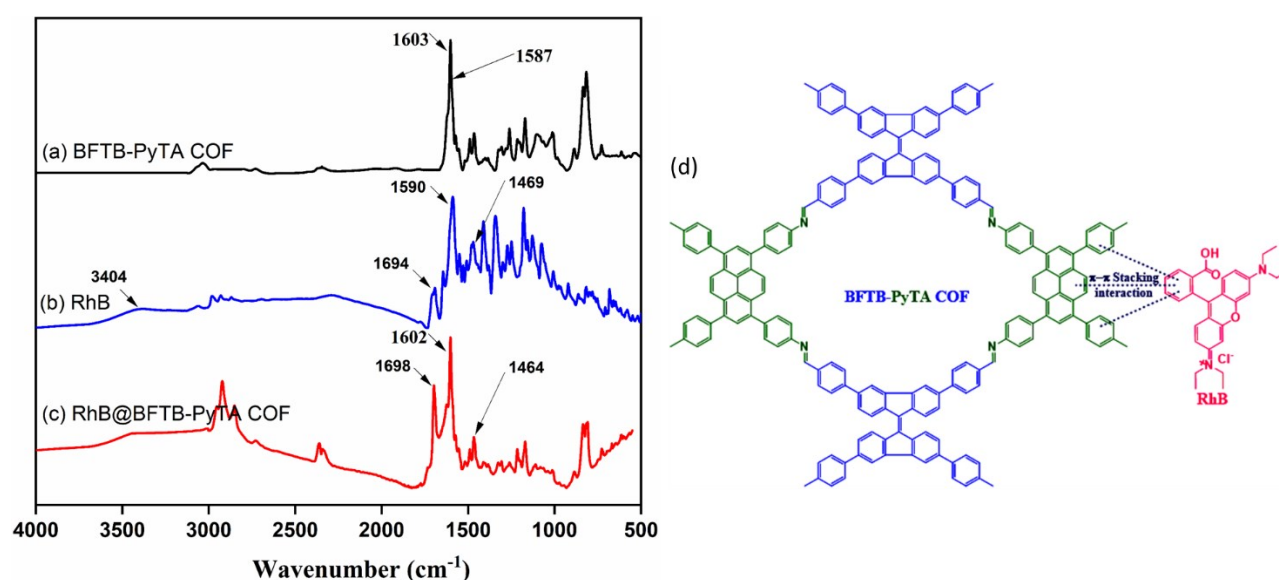


Figure S13. FT-IR spectra of (a) BFTB-PyTA COF, (b) rhodamine B (RhB), and (c) BFTB-PyTA COF after adsorbed rhodamine B. (d) Adsorption mechanism of rhodamine B on BFTB-PyTA COF.

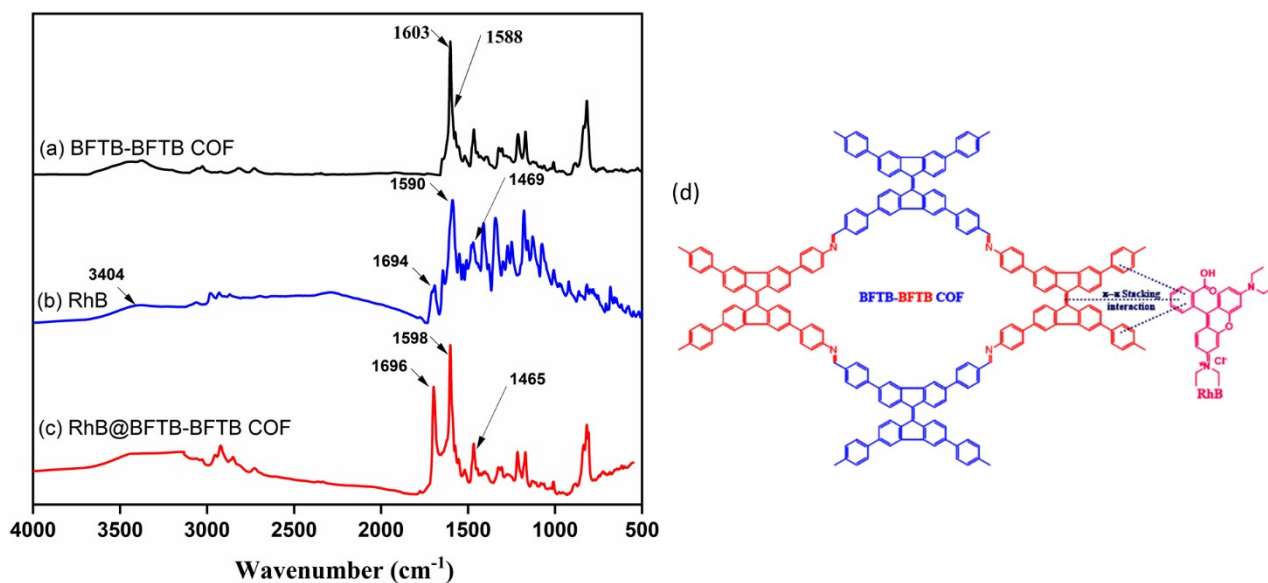


Figure S14. FT-IR spectra of (a) BFTB-BFTB COF, (b) rhodamine B (RhB), and (c) BFTB-PyTA COF after adsorbed rhodamine B. (d) Adsorption mechanism of rhodamine B on BFTB- BFTB COF.

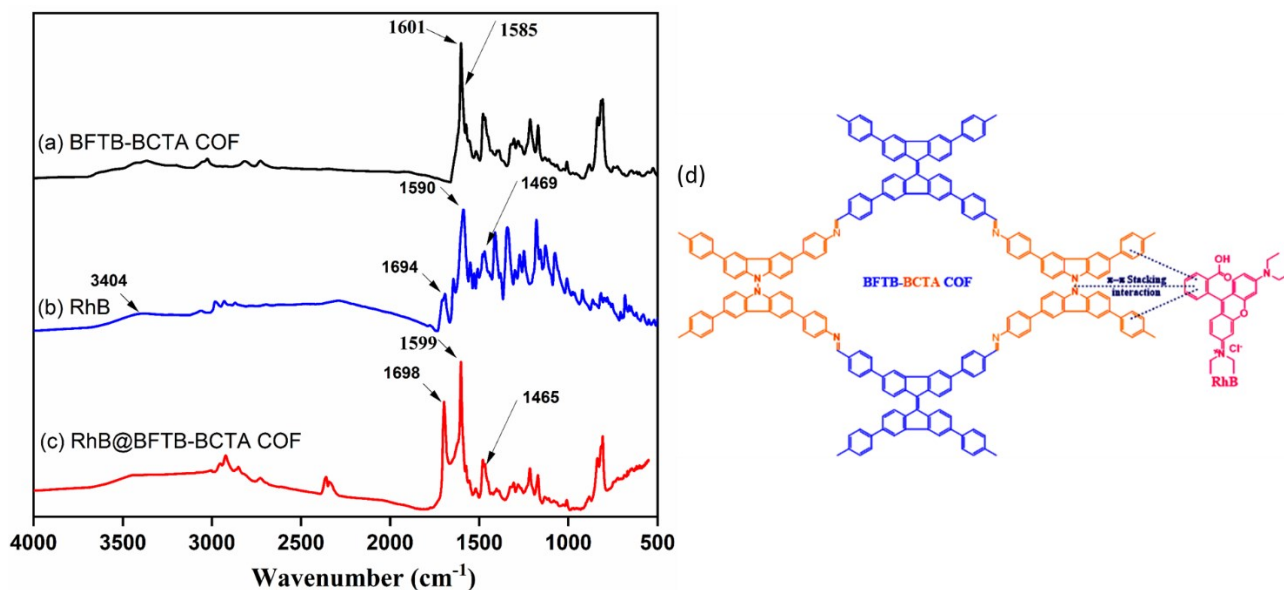
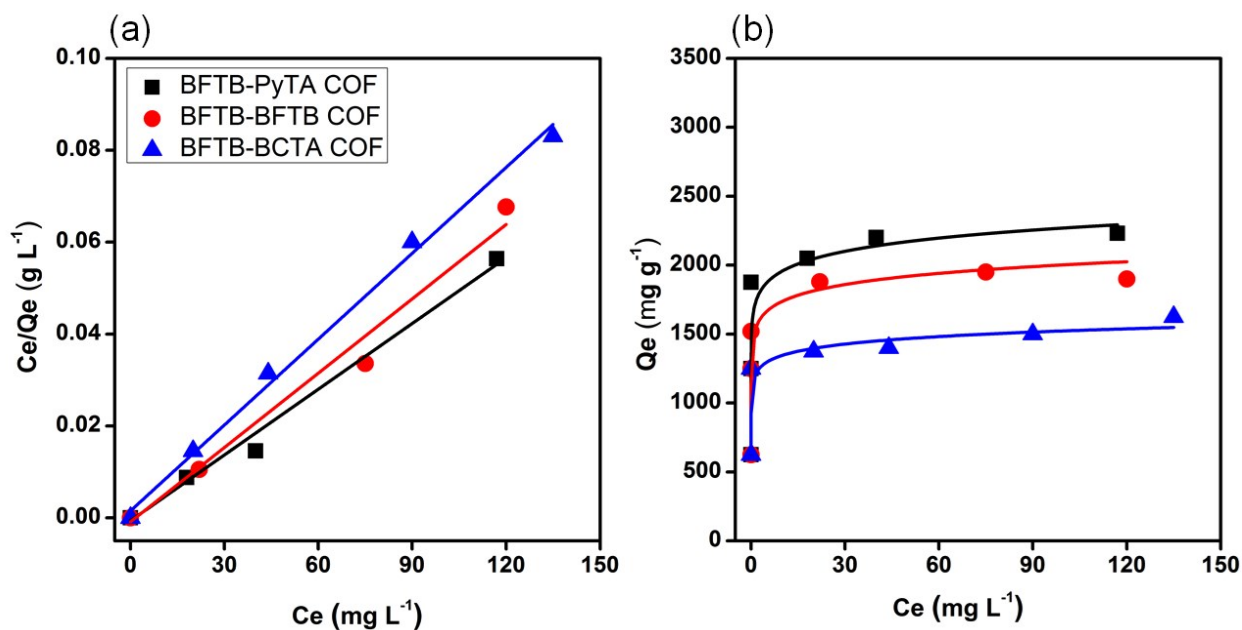
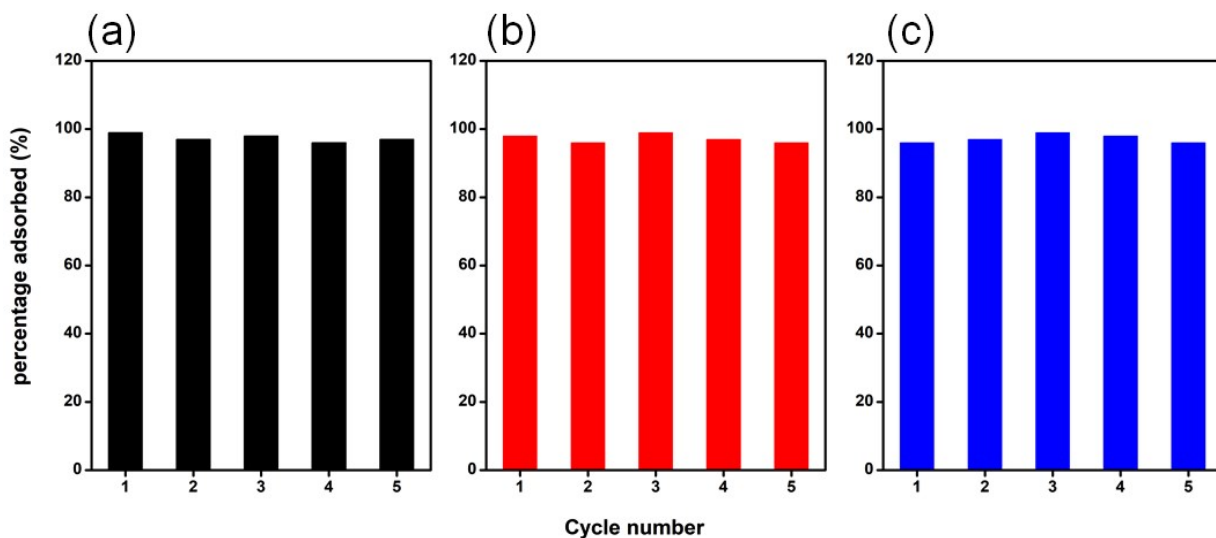


Figure S15. FT-IR spectra of (a) BFTB-BCTA COF, (b) rhodamine B (RhB), and (c) BFTB-PyTA COF after adsorbed rhodamine B. (d) Adsorption mechanism of rhodamine B on BFTB- BCTA COF.



F

Figure S16. (a) Langmuir isothermal models and (b) adsorption isothermal curves for RhB on the BFTB-PyTA, BFTB-BFTB, and BFTB-BCTA COFs.



Fig

Figure S17. Reusability of the (a) BFTB-PyTA, (b) BFTB-BFTB, and (c) BFTB-BCTA COFs for the removal of RhB within 10 min.

Table S6. Fitted parameters for the adsorptions of RhB on the BFTB-PyTA, BFTB-BFTB, and BFTB-BCTA COFs, calculated using the Langmuir adsorption isothermal model.

	Q_m (mg g ⁻¹)	K_L	R_L^2
BFTB-PyTA COF	2127	0.7580	0.9903
BFTB-BFTB COF	1854	0.6227	0.9891
BFTB-BCTA COF	1605	0.4127	0.9949

Table S7. Maximum adsorption capacities of RhB on the BFTB-PyTA, BFTB-BFTB, and BFTB-BCTA COFs, compared with those of other reported materials.

Adsorbent	Dye	Q_m (mg g ⁻¹)	Ref.
Graphene sponge	RhB	72	S5
Nanoporous PDVB-VI-0.2	RhB	260	S6
S1	RhB	200	S7
activated carbon (OAC)	RhB	321	S8
Mesoporous carbon (ST-A)	RhB	83	S9
N-doped mesoporous gyroid carbon	RhB	204.08	S10
PDVB-VI nanoporous polymer	RhB	260	S11
CMP-YA	RhB	535	S12
Py-BF-CMP	RhB	1905	S13
TPE-BF-CMP	RhB	1024	S13
TPA-BF-CMP	RhB	926	S13
Ttba-TPDA-COF	RhB	833	S14
CuP-DMNDA-COF/Fe	RhB	424	S15
BFTB-PyTA	RhB	2127	This work
BFTB-BFTB	RhB	1854	This work
BFTB-BCTA	RhB	1605	This work

S12. Chemical stability of COFs

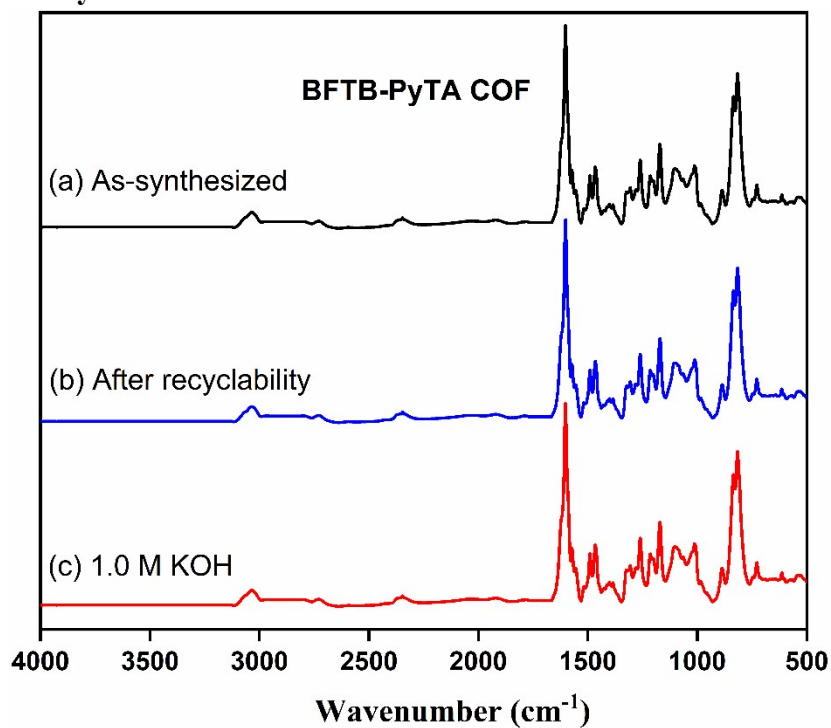


Figure S18. FTIR spectra of BFTB-PyTA COF (a) as-synthesized, (b) after recyclability from dye experiments and (c) after immersing 3 days in 1.0 M KOH.

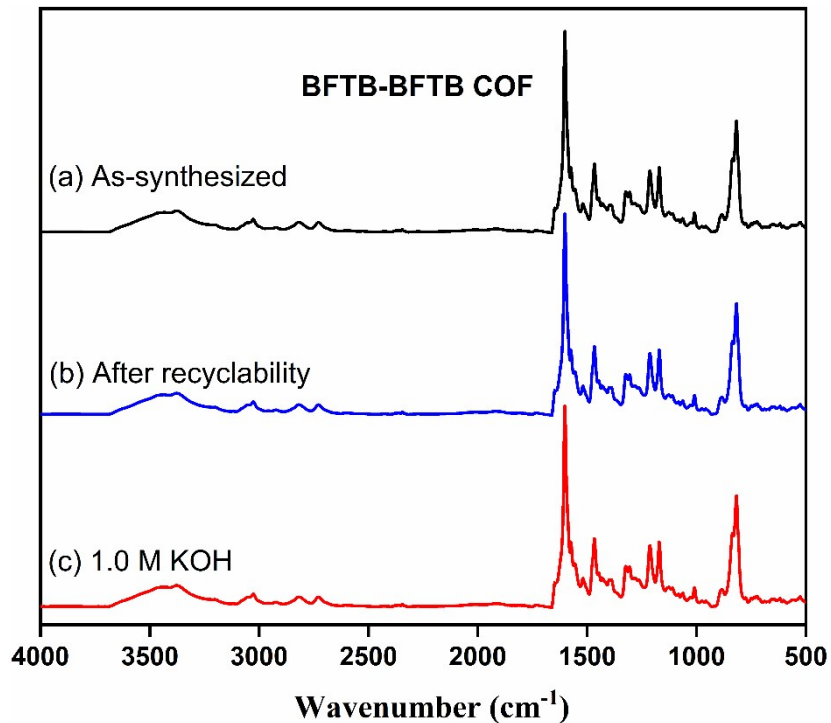


Figure S19. FTIR spectra of BFTB-BFTB COF (a) as-synthesized, (b) after recyclability from dye experiments and (c) after immersing 3 days in 1.0 M KOH.

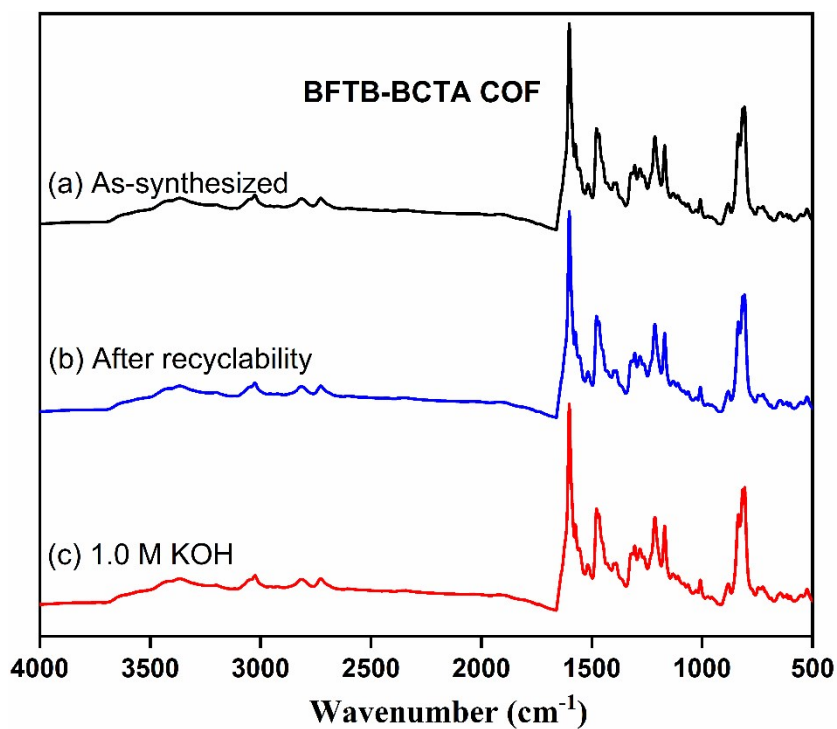


Figure S20. FTIR spectra of BFTB-BCTA COF (a) as-synthesized, (b) after recyclability from dye experiments and (a) after immersing 3 days in 1.0 M KOH.

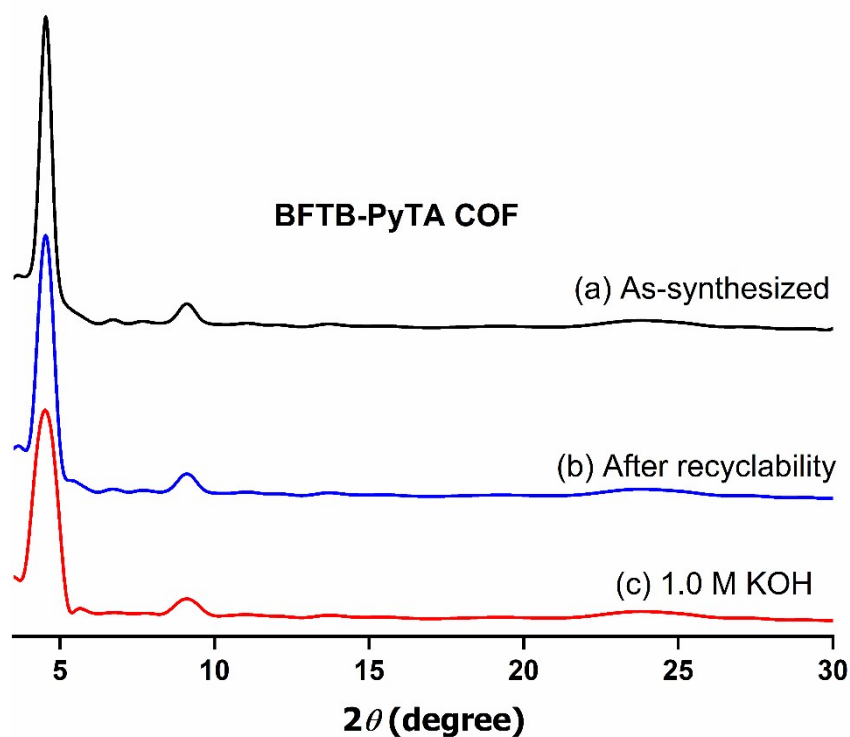


Figure S21. PXRD patterns of BFTB-PyTA COF (a) as-synthesized, (b) after recyclability from dye experiments and (a) after immersing 3 days in 1.0 M KOH.

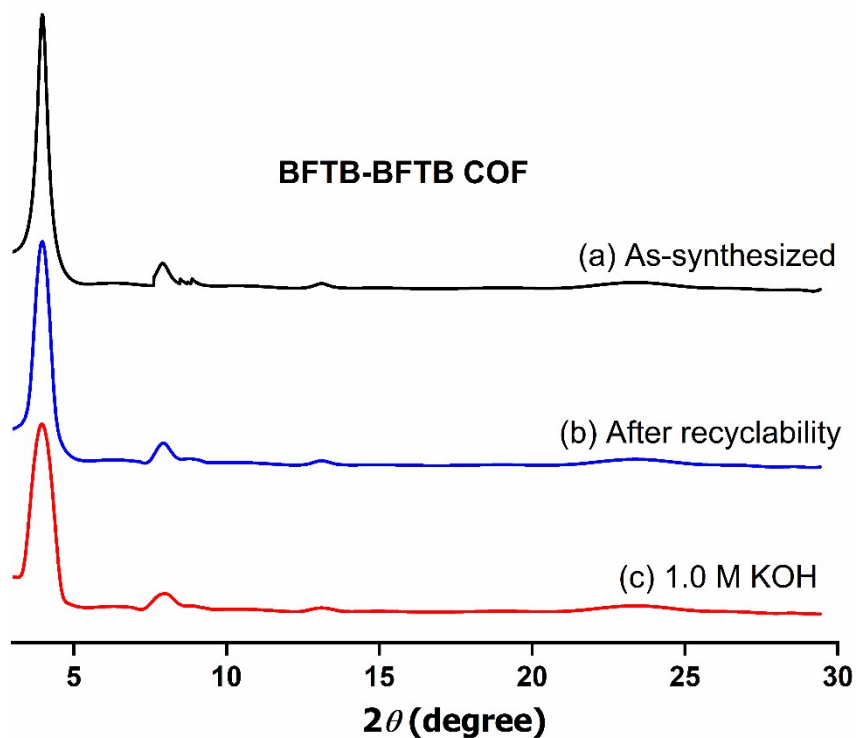


Figure S22. PXRD patterns of BFTB-BFTB COF (a) as-synthesized, (b) after recyclability from dye experiments and (c) after immersing 3 days in 1.0 M KOH.

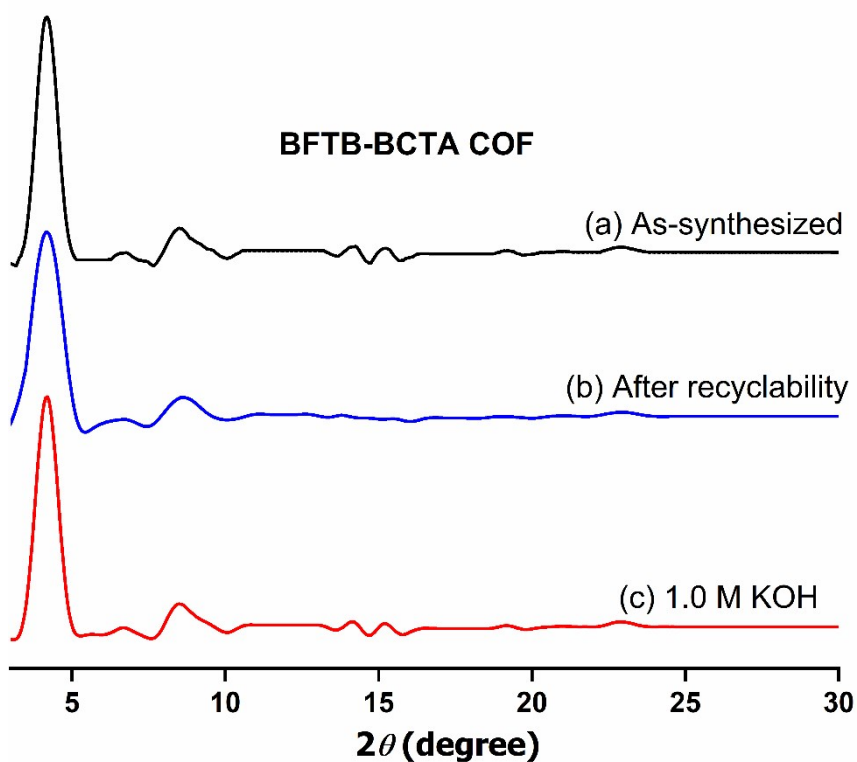


Figure S23. PXRD patterns of BFTB-BCTA COF (a) as-synthesized, (b) after recyclability from dye experiments and (c) after immersing 3 days in 1.0 M KOH.

S13. Electrochemical measurements

All electrochemical measurements were performed using an Autolab potentiostat (PGSTAT204) in a three-electrode electrochemical cell. The performance of the electrodes was investigated through cyclic voltammetry (CV) and the galvanostatic charge-discharge (GCD) method in 1.0 M KOH as the electrolyte. A Pt wire was used as the counter electrode; Ag/AgCl was used as the reference electrode; a glassy carbon electrode (GCE) was used as the working electrode (diameter: 5.61 mm; 0.2475 cm²). Prior to use, the GCE was polished several times sequentially with 0.1- and 0.05- μ m alumina powder, washed with distilled water and EtOH after each polishing step, cleaned via sonication (5 min) in a water bath, washed with EtOH, and finally dried under a stream of N₂.

The working electrode was prepared by coating a slurry containing the active material. The slurry was prepared by dispersing the active material (2.0 mg), carbon black (2.0 mg), and Nafion (0.4 mg) in EtOH (1.0 mL), which had undergone sonication for 1 h. A portion of the freshly prepared slurry (10 μ L) was coated onto the tip of the electrode, then dried in air for 30 min prior to use. The electrochemical performance was studied through CV at various sweep rates (from 5 to 200 mV s⁻¹) and through the GCD method in the potential range from -1.0 to 0.0 V (vs. Ag/AgCl) at various current densities (from 0.5 to 20 A g⁻¹) in 1 M KOH as the aqueous electrolyte. The specific gravimetric capacitance of each electrode was calculated from the CV curves by using the following equation (1):

$$C_g = \frac{1}{ms(V_f - V_i)} \int_{V_i}^{V_f} I(V)dv \quad (1)$$

where C_g is the gravimetric capacitance (F g⁻¹), s is the potential scan rate, V is the potential window, I is the current (A), t is the discharge time (s), and m is the mass of the active material (g).

Based on the GCD data, the gravimetric specific capacitance (C_g , F g⁻¹) was calculated using the following equation (2):

$$C_g = \frac{I \times t}{m \times \Delta V} \quad (2)$$

where I is the discharge current (A), t is the discharge time (s), m is the mass of the active material (g), and ΔV is the potential change during the discharge process (V).

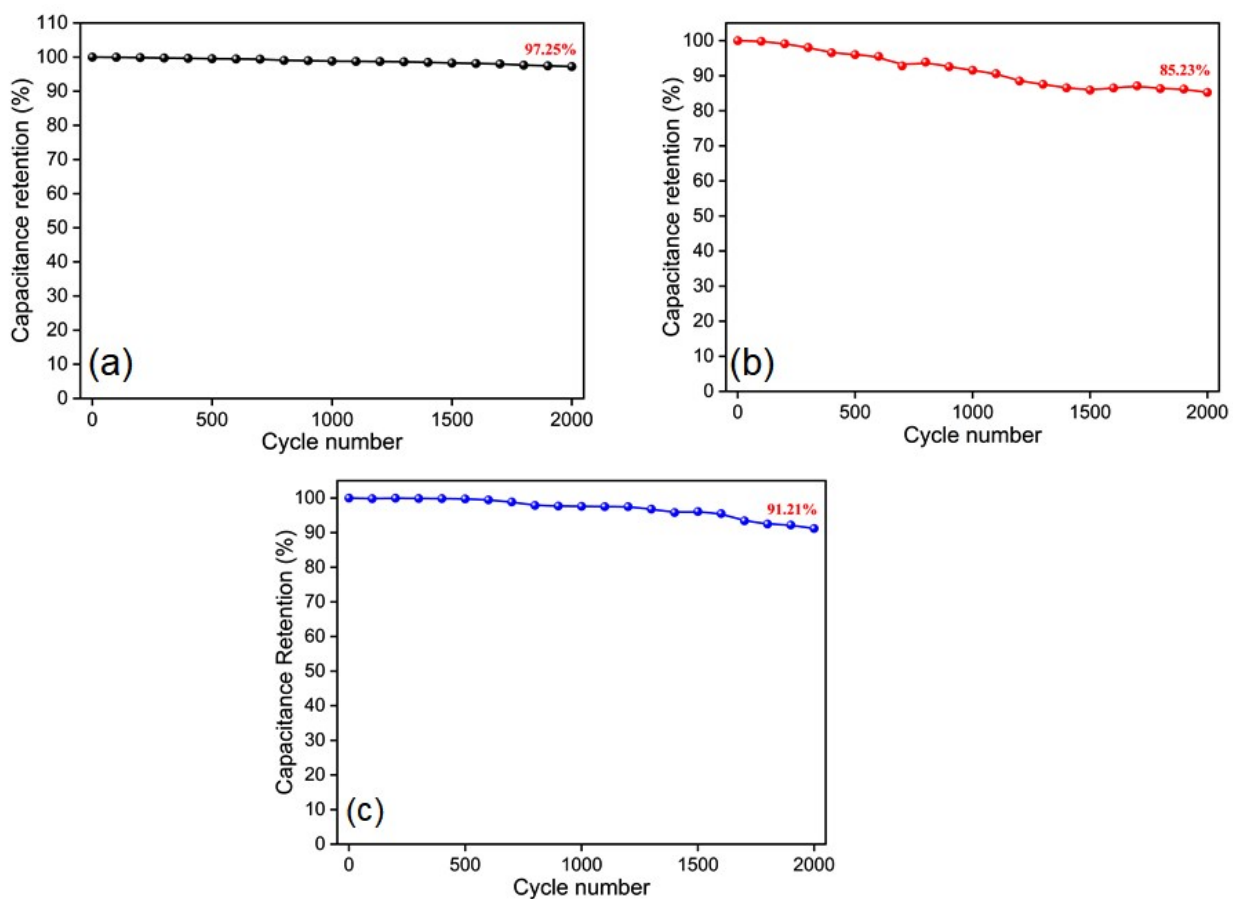


Figure S24. Cycling performances of a) BFTB-PyTA, b) BFTB-BFTB and c) BFTB-BCTA electrodes at 10 A g^{-1} .

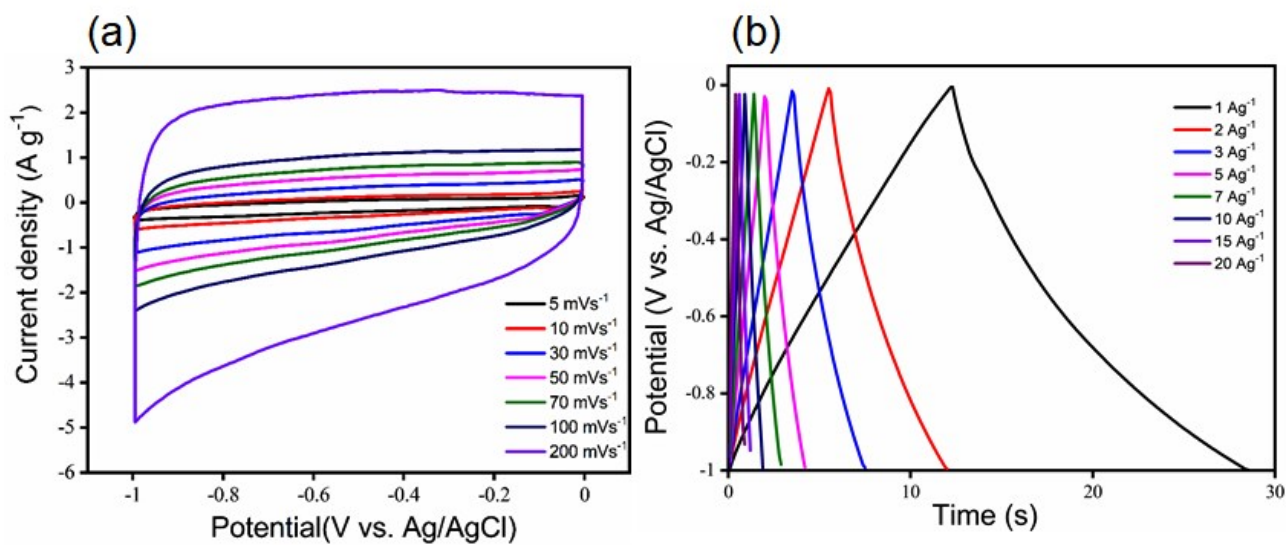


Figure S25. (a) CV curves and (b) GCD curves of black carbon.

Table S8. Gravimetric specific capacitance values calculated at different scan rates and retention.

	Scan rate (mV s ⁻¹)	Discharge area (cm ²)	C _g (F g ⁻¹)	Retention (%)
BFTB-PyTA	5	0.068	68.0	52.9
	10	0.119	59.5	
	30	0.295	49.1	
	50	0.451	45.1	
	70	0.598	42.7	
	100	0.805	40.3	
	200	1.410	35.3	
BFTB- BFTB	5	0.084	84.5	47.7
	10	0.148	74.2	
	30	0.377	62.8	
	50	0.574	57.5	
	70	0.754	53.8	
	100	0.992	49.5	
	200	1.613	40.3	
BFTB-BCTA	5	0.089	89.9	47.4
	10	0.145	72.6	
	30	0.339	56.5	
	50	0.523	52.3	
	70	0.697	49.7	
	100	0.943	47.1	
	200	1.707	42.6	

Table S9. Comparison between the specific surface area/specific capacitance of BFTB-PyTA, BFTB-BFTB, and BFTB-BCTA COFs with those of previously reported COFs for supercapacitor application.

COFs	S_{BET} ($\text{m}^2 \text{g}^{-1}$)	Capacitance	Ref.
Car-TPA COF	1334	13.6 F g^{-1} at 0.2 A g^{-1}	S16
Car-TPP COF	743	14.5 F g^{-1} at 0.2 A g^{-1}	S16
Car-TPT COF	721	17.4 F g^{-1} at 0.2 A g^{-1}	S16
DAAQ-TFP COF	1280	48 \pm 10 F g^{-1} at 0.1 A g^{-1}	S17
TPA-COF-1	714	51.3 F g^{-1} at 0.2 A g^{-1}	S18
TPA-COF-2	478	14.4 F g^{-1} at 0.2 A g^{-1}	S18
TPA-COF-3	557	5.1 F g^{-1} at 0.2 A g^{-1}	S18
TPT-COF-4	1132	2.4 F g^{-1} at 0.2 A g^{-1}	S18
TPT-COF-5	1747	0.34 F g^{-1} at 0.2 A g^{-1}	S18
TPT-COF-6	1535	0.24 F g^{-1} at 0.2 A g^{-1}	S18
TaPay-Py COF	687	209 F g^{-1} at 0.5 A g^{-1}	S19
DAB-TFP COF	385	98 F g^{-1} at 0.5 A g^{-1}	S19
TPT-DAHQ COF	1855	256 F g^{-1} at 0.5 A g^{-1}	S20
PDC-MA COF	748	335 F g^{-1} at 1.0 A g^{-1}	S21
TpPa-(OH) ₂ COF	369	416 F g^{-1} at 1.0 A g^{-1}	S22
BFTB-PyTA COF	1133	71 F g^{-1} at 1 A g^{-1}	This work

S14. Reference

- [S1] K. Brunner, A. V. Dijken, H. Borner, J. J. A. M. Bastiaansen, N. M. M. Kiggen and B. M. W. Langeveld, *J. Am. Chem. Soc.*, 2004, **126**, 6035-6042.
- [S2] J. Ipaktschi, R. Hosseinzadeh, P. Schlaf and E. Dreiseidler, *Helv. Chim. Acta.*, 1998, **81**, 1821-1834.
- [S3] P. Rios, T. S. Carter, T. J. Mooibroek, M. P. Crump, M. Lisbjerg, M. Pittelkow, N. T. Supekar, G. J. Boons and A. P. Davis, *Angew. Chem. Int. Ed.*, 2016, **55**, 3387-3392.
- [S4] H. R. Abuzeid, A. F. M. EL-Mahdy and S. W. Kuo, *Microporous Mesoporous Mater.*, 2020, **300**, 110151.
- [S5] J. Zhao, W. Ren and H. M. Cheng, *J. Mater. Chem.*, 2012, **22**, 20197-20202.
- [S6] Y. Han, W. Li, J. Zhang, H. Meng, Y. Xu and X. Zhang, *RSC Adv.*, 2015, **5**, 104915-104922.
- [S7] S. Wang, B. Yang and Y. Liu, *J. Colloid Interface Sci.*, 2017, **507**, 225-233.
- [S8] O. Üner, Ü. Geçgel, H. Kolancılar and Y. Bayrak, *Chem. Eng. Commun.*, 2017, **204**, 772-783.
- [S9] K. Jedynak, D. Widel and N. Redzia, *Colloids Interfaces*, 2019, **3**, 30.
- [S10] A. F. M. EL-Mahdy, T. E. Liu and S. W. Kuo, *J. Hazard. Mater.*, 2020, **391**, 122163.
- [S11] Y. Han, W. Li, J. Zhang, H. Meng, Y. Xu and X. Zhang, *RSC Adv.*, 2015, **5**, 104915-104922.
- [S12] Y. Yuan, H. Huang, L. Chen and Y. Chen, *Macromolecules*, 2017, **50**, 4993-5003.
- [S13] B. Wang, Z. Xie, Y. Li, Z. Yang and L. Chen, *Macromolecules*, 2018, **51**, 3443-3449.
- [S14] T. Xu, S. An, C. Peng, J. Hu and H. Liu, *Ind. Eng. Chem. Res.*, 2020, **59**, 8315-8322.
- [S15] Y. Hou, X. Zhang, C. Wang, D. Qi, Y. Gu, Z. Wang, and J. Jiang, *New J. Chem.*, 2017, **41**, 6145-6151.
- [S16] A. F. M. El-Mahdy, C. Young, J. Kim, J. You, Y. Yamauchi and S. W. Kuo, *ACS Appl. Mater. Interfaces*, 2019, **11**, 9343-9354.
- [S17] C. R. DeBlase, K. E. Silberstein, T. T. Truong, H. D. Abruña and W. R. Dichtel, *J. Am. Chem. Soc.*, 2013, **135**, 16821-16824.
- [S18] A. F. M. El-Mahdy, C. H. Kuo, A. Alshehri, C. Young, Y. Yamauchi, J. Kim and S. W. Kuo, *J. Mater. Chem. A*, 2018, **6**, 19532-19541.
- [S19] A. M. Khattak, Z. A. Ghazi, B. Liang, N. A. Khan, A. Iqbal, L. Li and Z. Tang, *J. Mater. Chem. A*, 2016, **4**, 16312-16317.
- [S20] A. F. M. EL-Mahdy, Y. -H. Hung, T. H. Mansoure, H. -H. Yu, T. Chen, and S. W. Kuo, *Chem. Asian J.*, 2019, **14**, 1429-1435.
- [S21] L. Li, F. Lu, R. Xue, B. Ma, Q. Li, N. Wu, H. Liu, W. Yao, H. Guo, and W. Yang, *ACS Appl. Mater. Interfaces* 2019, **11**, 26355-26363.
- [S22] S. Chandra, D. R. Chowdhury, M. Addicoat, T. Heine, A. Paul, and R. Banerjee, *Chem. Mater.* 2017, **29**, 2074-2080.